

1 **Morphotectonics and Strain Partitioning at the Iberia-Africa plate boundary from**
2 **multibeam and seismic reflection data**

3

4 Terrinha, P.^(1,4), Matias, L.⁽²⁾, Vicente, J.^(1,3), Duarte, J.^(1,3), Luís, J.⁽⁵⁾, Pinheiro, L.⁽⁶⁾,
5 Lourenço, N.^(5,7), Diez, S.⁽⁸⁾, Rosas, F.⁽⁴⁾, Magalhães, V.⁽⁶⁾, Valadares, V.^(1,3), Zitellini,
6 N.⁽⁹⁾, Roque, C.^(1,7), Mendes Víctor, L.⁽²⁾ and MATESPRO Team

7

8 ⁽¹⁾ Laboratório Nacional de Energia e Geologia (LNEG), Unidade de Geologia Marinha,
9 Portugal; ⁽²⁾ Fac. Science Univ. Lisbon, Portugal (CGUL, IDL); ⁽³⁾ Câmara Municipal de
10 Lisboa; ⁽⁴⁾ Fac. Science Univ. Lisbon, Portugal (LATTEX, IDL); ⁽⁵⁾ Univ. Algarve,
11 CIMA, Portugal; ⁽⁶⁾ Universidade de Aveiro, CESAM, Portugal; ⁽⁷⁾ EMEPC; ⁽⁸⁾ Unidad
12 de Tecnología Marina (UTM-CSIC), Barcelona, Spain; ⁽⁹⁾ Istituto di Scienze Marine,
13 (ISMAR), Bologna, Italy.

14

15 MATESPRO Team: Teresa Medialdea, Marzia Rovere, Caterina Basile, Toni Bermudez

16

17 Corresponding author: Terrinha, P. – e-mail: pedro.terrinha@ineti.pt; fax:
18 +351 214 719 018; telf: +351 21 470 55 41; address: Department Marine Geology,
19 LNEG, Estrada da Portela, 2721-866 Amadora, Portugal

20

21 **Abstract**

22 The Gulf of Cadiz, off SW Iberia and the NW Moroccan margin, straddles the cryptic
23 plate boundary between Africa and Eurasia, a region where the orogenic Alpine
24 compressive deformation in the continental collision zone passes laterally to the west to

25 strike-slip deformation. A set of new multibeam bathymetry, multi-channel and single
26 channel seismic data presented here image the main morphological features of tectonic
27 origin of a significant part of the Gulf of Cadiz from the continental shelf to the abyssal
28 plain. These morphotectonic features are shown to result from the reactivation of deeply
29 rooted faults that changed their kinematics from the early Mesozoic rifting, through the
30 Late Cretaceous-Paleogene collision, to Pliocene-Quaternary thrusting and wrenching.
31 The old faults control deep incised, more than 100km long canyons and valleys. Several
32 effects of neotectonics on deep water seabed are shown. These include: i) the complex
33 morphology caused by wrenching on the 230 km long WNW-ESE faults that produced
34 en echelon folds on the sediments; ii) the formation of up to 5 km wide crescent shaped
35 scours at roughly 4 km water depth by reactivation of thrusts; iii) 10 km long creep
36 folds on the continental slope; and iv) the formation of landslides on active fault
37 escarpments. The present day deformation is partitioned on NE-SW thrusts and WNW-
38 ESE to W-E strike-slip faults and is propagating northwards on N-S trending thrusts
39 along the West Iberia Margin from 35.5°N to 38°N, which should be considered for
40 seismic hazard.

41

42 Keywords: Gulf of Cadiz; Southwest Iberia Margin. multibeam bathymetry,
43 morphotectonics, seismotectonics, wrench tectonics, strain partitioning, migration of
44 deformation.

45

46 **1. Introduction**

47 **1.1. Scope and objectives**

48 In recent years the Gulf of Cadiz (Fig. 1) has been recognized as a key site to
49 understand a broad spectrum of geological issues, such as: i) the tectonic evolution of

50 the Africa-Iberia plate boundary, the formation of the Gibraltar orogenic arc, the
51 earthquake and tsunamigenic structures, the origin of the catastrophic 1755 Lisbon
52 earthquake and tsunami (Argus et al., 1989; DeMets et al., 1994; Sillard et al., 1998;
53 Maldonado et al., 1999; Kreemer and Holt, 2001; Zitellini et al., 2001; Calais et al.,
54 2002; Gutscher et al., 2002; Sella et al., 2002; Calais et al., 2003; Fernandes et al., 2003;
55 Gràcia et al., 2003; Terrinha et al., 2003; Gràcia et al., 2003a; Medialdea et al., 2004;
56 Nocquet and Calais, 2004; Stich et al., 2006) , ii) the Mediterranean Outflow Water
57 (MOW) and its relation to sedimentation and climate changes (Ambar et al., 2002;
58 Voelker et al., 2006; Hernandez-Molina et al., 2003; Mulder et al., 2003; Somoza et al.,
59 2003); iii) fluid escape and mud volcanism (Pinheiro et al., 2003; Somoza et al., 2003;
60 Van Rensbergen et al., 2005; Pinheiro et al., 2006a), and chemosynthetic ecosystems
61 associated to cold seeps (Niemann et al., 2006).

62 Behind this diversity of processes affecting the geosphere, the biosphere and the
63 hydrosphere, is a complex geological evolution of the area throughout the Neogene. It is
64 now well established, after various studies based on seismic reflection profiles, sidescan
65 sonar and ground truthing, that the whole area is under compressive deformation. A
66 number of active tectonic structures with high tsunamigenic potential were mapped
67 (Gràcia et al., 2003; Terrinha et al., 2003; Zitellini et al., 2004) and various multilayered
68 complexes of hemipelagic-mass wasting deposits of Holocene and Pleistocene age were
69 imaged and dated (Vizcaino et al., 2006).

70 The morphology of the northeastern part of the Gulf of Cadiz was described by
71 Hernandez-Molina et al.(2003), Mulder et al.(2003) and Somoza et al.(2003). The
72 morphology of the southern part of this sector is clearly influenced by the
73 tectonomorphic processes associated with the deformation of the Gulf of Cadiz
74 accretionary wedge (Maldonado et al., 1999; Gutscher et al., 2002), as well as

75 gravitational processes (Gutscher et al., 2008), whilst in the northern part the shaping
76 processes are sedimentary, erosive and tectonic, associated with the MOW and to
77 diapiric ridges.

78 The objective of this work is to describe the morphology of the northwestern part of the
79 Gulf of Cadiz and discuss the morphogenetic processes in relation to the tectonic
80 deformation of the Alpine collision front and the Gloria transform fault. This is done
81 based on the interpretation of an original multibeam bathymetry data and seismic
82 reflection profiles

83

84 **1.2. Geological setting**

85 During Triassic through Early Cretaceous times the southern and western Iberian
86 margins underwent tectonic rifting, which led to oceanic break-up of the West Iberian
87 Margin from Barremian to Aptian times (Pinheiro et al., 1996). Although the existence
88 of oceanic lithosphere in the Gulf of Cadiz is still a matter of debate (Srivastava et al.,
89 1990; Rovere et al., 2004; Gràcia et al., 2003), some authors postulated the existence of
90 a south Iberia subduction zone that accommodated the Africa-Iberia convergence, from
91 Late Cretaceous-Paleogene through Miocene times (e.g. Srivastava et al., 1990).
92 Accordingly, this process led to the formation of back arc basins and associated tectonic
93 terranes in the western Mediterranean, the formation of the Betic orogen, as well as to
94 the tectonic inversion of the rifted autochthonous south Portuguese and south Spanish
95 margins (e.g. Terrinha, 1998; Maldonado et al., 1999; Rosenbaum et al., 2002; Lopes et
96 al., 2006). Westward-directed thrusting of the Internal Betics domains and orogenic
97 collapse, possibly associated with roll back of the Africa subducted slab, formed the
98 Gibraltar orogenic arc, the Gulf of Cadiz accretionary wedge and lithospheric thinning
99 in the Alboran Sea (Rosenbaum et al., 2002; Faccenna et al., 2004). These tectonic

100 processes led to the formation of an accretionary wedge westward of the Gibraltar arc
101 (Gutscher et al., 2002) or imbricate wedge with a westward directed tectonic transport,
102 and an associated distal olistostrome complex (e.g., Horseshoe Gravitational Unit in
103 Iribarren et al., 2007; Giant Chaotic Body in Torelli et al., 1997) that extends across the
104 Horseshoe Abyssal Plain (fig. 2). The MCS lines reveal a basal decollement horizon of
105 the stacked thrusts of the accretionary wedge near the top of the Cretaceous. Both the
106 accretionary prism and the olistostrome are sealed by sediments of Late Miocene to
107 Lower Pliocene age (Tortella et al., 1997; Torelli et al., 1997; Roque, 2007). The
108 segment of the Azores-Gibraltar Fracture Zone to the east of the Gloria Fault (inset in
109 fig. 1) was described by Sartori et al. (1994) as a diffuse plate tectonic boundary and
110 various plate kinematic models indicate a 4mm/yr rate of NW-SE to WNW-ESE
111 convergence between Nubia and Iberia along this fault (insets in Figs.1 and 7), (Argus
112 et al., 1989; DeMets et al., 1994; Sillard et al., 1998; Kreemer and Holt, 2001; Calais et
113 al., 2002; Sella et al., 2002; Calais et al., 2003; Fernandes et al., 2003; Nocquet and
114 Calais, 2004; Stich et al., 2006). Ribeiro et al. (1996) postulated the formation of an
115 incipient West Iberia subduction zone during Pliocene-Quaternary times, based on the
116 computed NW-SE Present day main compression direction.
117 N-S to NE-SW faults formed in the Permian during the late Variscan fracturing event
118 (Arthaud and Matte, 1977; Ribeiro, 2002) and they were subsequently reactivated
119 during the Mesozoic rifting, the Mesozoic transient compressive episodes (Terrinha et
120 al., 2002) and the Cenozoic through Present compression (Fig. 2, Dias, 2001; Carrilho
121 et al., 2004).
122 Offshore, the N-S trending Marquês de Pombal and Pereira de Sousa faults lie on the
123 north to south trending southernmost segment of the West Iberian Margin. These faults
124 were described as active in the Quaternary by Zitellini et al. (1999), Zitellini et al.

125 (2001), Gràcia et al. (2003) and Terrinha et al. (2003). The uneven surface of the
126 Marquês de Pombal fault scarp is due to widespread slumping and landslides with mass
127 transport distances that exceed 20 km. The Pereira de Sousa fault scarp is also heavily
128 incised and the D. Henrique basin shows a series of radial ridges that consist of turbidite
129 levees transported down slope from the highs that surround it (Gràcia et al., 2003;
130 Terrinha et al., 2003).

131 WSW-ENE to W-E trending Mesozoic rifting faults were inverted during the latest
132 Cretaceous through early Miocene times (Terrinha, 1998; Lopes et al., 2006).
133 Duarte et al. (2005) showed the existence of presently active WNW-ESE trending faults
134 in the Gulf of Cadiz and Medialdea et al. (2007) proposed that these faults acted as
135 transfer faults between the Gorringe Bank and the Marquês de Pombal fault across the
136 Horseshoe fault. Onshore southwest Portugal, WNW-ESE trending Lower Jurassic
137 extensional faults were described by Ribeiro and Terrinha (2007). Zitellini et al. (2009)
138 proposed the existence of a Nubia-Eurasia plate boundary based on a set of 600 km long
139 WNW-ESE trending set of strike-slip faults that cut across the Horseshoe Abyssal Plain
140 and Gulf of Cadiz connecting the Gloria Fault and the Tell tectonic zone onshore north-
141 west Morocco.

142 Earthquake frequency and epicentre location (Fig. 2) show that SW Iberia is an area of
143 moderate seismicity which accommodates the brittle deformation associated with the
144 Nubia-Iberia collision west of Gibraltar, by means of thrusting and strike-slip events of
145 shallow and intermediate depth. However, the existence of historical and instrumental
146 high magnitude earthquakes such as the 1/11/1755 Lisbon earthquake ($M=8.5$ to 8.9)
147 and the 28/2/1969 ($M_s=7.9$) event require clarification of the present tectonic setting of
148 the SW Iberia-NW Africa region, and identification of the structures that generate large
149 magnitude earthquakes and tsunamis in this area. The Gorringe Bank Fault is a north

150 westwards directed thrust that sits at the northern base of this morphologic feature. This
151 thrust uplifted the seafloor from approximately -5000 m to -24 m, it reached its
152 paroxysmal activity in Miocene times and has accommodated negligible shortening
153 since then (Sartori et al., 1994; Tortella et al., 1997). Although the Gorringe Bank is by
154 far the most conspicuous morphotectonic structure in the study area (Fig. 1), the
155 distribution of seismicity (Fig. 2), numerical models for tsunami wave propagation
156 (Baptista et al., 1998) and the interpretation of MCS lines (Sartori et al., 1994), led
157 various researchers to abandon it as the source of the 1755 Lisbon earthquake.
158 Recent models proposed the existence of two faults, the Marquês de Pombal Fault and
159 the Horseshoe fault (Gràcia et al., 2003; Terrinha et al., 2003) (Fig. 2) or the Marquês
160 de Pombal Fault and the Guadalquivir Bank fault (Baptista et al., 2003), acting together
161 simultaneously to generate the 1755 event by adding up their rupture areas (Baptista et
162 al., 2003; Gràcia et al., 2003; Terrinha et al., 2003). Alternatively, Gutscher et al. (2002)
163 proposed that the 1755 Lisbon earthquake was generated in the Gibraltar subduction
164 zone imaged on seismic tomography, arguing that this was also the source of the deep
165 1954 Granada earthquake.

166

167 **1.3. Data and methods**

168 38.000 km² of multibeam swath bathymetry data were acquired in the MATESPRO
169 Survey with a hull-mounted Simrad EM 120 echo-sounder aboard the research vessel
170 NRP D. Carlos I in 3 legs from 14 June to 7 July 2004 (Figs. 3 and 4). The survey was
171 carried out in order to comply with a level 3 hydrographic survey as established by the
172 International Hydrographic Organization. The EM 120 operates at a main frequency of
173 12 kHz (from 11.25 to 12.6 kHz) with 191 beams covering a 150° degrees fan with a
174 width of 1°. In order to increase data quality the angular value was reduced to 120

175 degrees and the ping width was of 2 degrees. One Sound Velocity Profile (SVP) was
176 performed every 24 hours and at locations chosen to spatially cover the entire area in
177 order to compensate the effect of the Mediterranean Outflow Water on the sound
178 velocity in the water column regionally. SVP data were acquired down to 2000 m of
179 water depth. From -2000 to -4000 m sound velocity was taken from climatologic
180 profiles provided by the Instituto Hidrográfico of Portugal in this area. Quality control
181 lines were also performed totalizing about 10% of the area; the depth errors found were
182 below 0.3% of the water depth. Bathymetric data filtering and processing was carried
183 using CARIS HIPS software and a 100m grid was generated.

184 The positioning of the vessel was done with both GPS and DGPS mounted on different
185 parts of the vessel in order to better determinate the position and make the yaw
186 corrections; the errors associated with the navigation positioning were around 5 meters.
187 The seismic data presented here are of two types: multichannel seismic (MCS) profiles
188 from three previous surveys, ARRIFANO (acronym of Arco Rifano; Sartori et al.,
189 1994), IAM (acronym of Iberian Atlantic Margin; Banda et al., 1995) and VOLTAIRE
190 (acronym of Valuation Of Large Tsunamis And Iberian Risk for Earthquakes) and one
191 single-channel profile acquired during the TTR-14 survey (Training Through Research;
192 Kenyon et al., 2006).

193 The IAM and ARRIFANO deep MCS have a similar central peak frequency of
194 approximately 30 Hz and the VOLTAIRE MCS has a central peak frequency of
195 approximately 50 Hz. As a result, the vertical resolution in the sedimentary section is of
196 around 20 meters for the IAM and ARRIFANO profiles and of about 15 meters for the
197 VOLTAIRE data, assuming a mean seismic velocity of 2500 ms^{-1} in the sedimentary
198 section (data from bore-holes in Fig. 3 and Gonzalez et al., 1998). The central peak
199 frequency of the single channel TTR profile is around 100 Hz with a corresponding

200 vertical resolution of about 6 meters. Information on acquisition and processing of these
201 profiles is summarized in Table 1.

202 (Table 1)

203

204 The presented seismostratigraphic interpretation was based on the stratigraphy of five
205 industry wells offshore the Algarve Basin (stars in Fig. 1, Lopes et al., 2006), as well as
206 published data from the offshore Guadalquivir Basin (Maldonado et al., 1999).

207

208 **2. Morphology of the NW part of the Gulf of Cadiz**

209 The MATESPRO multi-beam dataset (Fig. 4) shows a variety of seafloor major
210 morphological features within which smaller scale features indicative of genetic
211 processes discussed elsewhere in this paper are found.

212

213 **2.1. The submarine sediment drainage system**

214 The drainage system of the study area is subdivided in two groups: a northern one that
215 drains the Portuguese continental margin from north to south, and a southern one that
216 drains the western continental shelf of Spain.

217 **2.1.1. The north to south sediment drainage system**

218 The north to south oriented drainage system consists of a poorly organized network of
219 gullies and canyons. The deeply incised 120 km long São Vicente canyon (Fig. 1) has
220 its head scarp at 70m below sea level (mbsl), cuts across the shelf and slope and ends in
221 the Horseshoe Abyssal Plain. The maximum incision into the sedimentary substratum
222 on the continental slope is of 2 km. This canyon is made up of two segments oriented
223 NE-SW and N-S that collect the sediment from the gullies that incise the shelf and slope

224 (Figs. 4 and 5). Also note that the flanks of the NE-SW trending segment and the
225 eastern flank of the N-S trending segment display higher degree of incision, whilst the
226 western flank of the N-S trending segment and both flanks of the deepest part of the
227 canyon are smoother. The close up in Fig. 6A shows a submarine landslide near the
228 termination of the canyon. The lack of the mass transport deposit within the canyon is
229 an indication of the activity of the canyon in terms of sediment erosion and transport.

230 The 70 km long Portimão canyon also has its head scarp in the shelf at roughly 70 mbsl.
231 The canyon cuts across the shelf and slope sedimentary sequence with a maximum
232 incision of 1 km. The canyon terminates abruptly at the meeting point with the Faro
233 canyon and D. Carlos valley that drain east to west. These features have a different
234 physiography, with a flat and broad bottom capable of accommodating larger sediment
235 influx. The Portimão canyon is fairly rectilinear and sits along the Portimão Fault
236 (Terrinha et al., 1999).

237 The Aljezur and Lagos canyons only incise the continental slope. The NNE-SSW
238 trending Aljezur canyon is short, rectilinear and drains into the Sagres valley. The
239 western flank of the Aljezur canyon displays a series of anastomosed submarine slide
240 scars at approximately 1300 mbsl, at a main morphologic break of the continental slope
241 near the base of the Lagos contourite drift (Fig. 6B).

242 The Sagres valley collects the east to west draining D. Carlos and Cadiz valleys and the
243 Aljezur and Lagos canyons. The Aljezur canyon and Sagres valley lie on the southern
244 prolongation of an important slope break that can be observed in the low resolution
245 bathymetry (see Figs. 2, 4 and 5) and also on the southern continuation of the Aljezur
246 Fault that cuts across the Meso-Cenozoic Algarve Basin and Paleozoic basement (Fig.
247 2).

248 The Lagos canyon has its head scarp roughly at 800 mbsl, where it incises the Pliocene
249 through Holocene Lagos contourite drift.

250 **2.1.2. East to west oriented sediment drainage system**

251 The seafloor of the inner part of the Gulf of Cadiz dips to the west towards the Atlantic
252 Ocean. The seafloor is shaped by a variety of morphological features of various scales,
253 many of which have been described by Mulder et al. (2003), Somoza et al. (2003),
254 Molina-Hernandez et al. (2006), Gutscher et al. (2008).

255 The most important E-W trending valleys of the study area lie in the prolongation of the
256 sinuous and broader E-W channels that initiate on the Gibraltar Arc owing to erosion
257 and sedimentation by the MOW and to down-slope gravity processes (Hernandez-
258 Molina et al., 2003). In the study area these valleys are broad, with flat gently dipping
259 bottom. The Faro canyon and D. Carlos valley collect the sediment transport from the
260 South Portuguese margins, a large number of gullies, valleys and the Portimão canyon.
261 The D. Carlos valley changes from narrow channel to broad valley downslope from the
262 merge of the Portimão Canyon..

263 The Cadiz valley lies between the Portimão Bank and the wrinkled surface of the Gulf
264 of Cadiz accretionary wedge. The Sagres valley that lies in the prolongation of the
265 Aljezur canyon establishes the connection between the drainage system located to the
266 east of the Horseshoe Fault scarp and the Horseshoe Abyssal Plain. The Sagres valley
267 displays a corrugate bottom north of the confluence with the Cadiz valley; from this
268 point to the south it has a smooth surface and less dip. The flanks of the Sagres valley
269 display various evidences of gravity slumping (Fig. 6B).

270 The Horseshoe valley is a roughly rectangular area, 80 km x 50 km, dipping to the west
271 (mean dip of $\sim 0.5^\circ$), connecting the Gulf of Cadiz seafloor and the Horseshoe Abyssal

272 Plain across the Horseshoe Fault scarp (Fig. 1). The valley is limited by the Sagres
273 plateau in the north, the Coral Patch Ridge in the south and the Gulf of Cadiz
274 accretionary wedge in the east. It is cross cut by WNW-ESE trending morphological
275 lineaments described elsewhere in this paper. This wide valley collects the mouths of
276 well developed canyons and valleys that drain the sediments from the north and eastern
277 shelves. The drainage to the Horseshoe Abyssal Plain is poorly developed (Fig. 5) and
278 the Horseshoe fault scarp is being eroded in various segments showing evidences of
279 landsliding (Fig. 6C). These different styles and degrees of maturation of the sediment
280 drainage pattern suggest that this area acts simultaneously as a by-pass and receptacle
281 region for the sediments that are carried from the continental shelves to the Horseshoe
282 Abyssal Plain.

283 Despite the general low slope of this area, there are NE-SW trending scarps with a
284 maximum height of approximately 150 m (Fig. 7). The flat areas have maximum dips of
285 3° and slope breaks in which formed convex upwards crescent shaped escarpments. The
286 crescent shaped three-dimensional features measure up to 5km across, are shown in
287 detail in Fig. 7 to occur between 3900 and 4700mbsl, have an internal escarpment up to
288 ~100m high with an internal slope varying from 6° to 27° .

289 **2.2. Plateaus and escarpments**

290 The plateaus in the study area are the Marquês de Pombal, Sagres and Portimão plateaus
291 (Figs. 1, 4 and 5). The Marquês de Pombal plateau is a roughly rectangular surface
292 bound by the NNE-SSW trending Marquês de Pombal reverse fault scarp in the west
293 and by the São Vicente canyon in the east, as described by Gràcia et al. (2003).

294 The Sagres plateau has an approximately rectangular shape divided by a diagonal NE-
295 SW trending crest. To the west, the Sagres plateau is bound by the Horseshoe reverse

296 fault scarp and the São Vicente canyon and by the Aljezur canyon and the Sagres Valley
297 in the east. In the north this plateau is separated from the mid and upper continental
298 slope and shelf by a rectilinear E-W trending valley that lies in the prolongation of the
299 D. Carlos valley.

300 The Horseshoe fault scarp is only well developed on its northern segment. The southern
301 part is being eroded (Fig. 6C) by the sediment drainage system described previously.

302 The southern part of the Sagres plateau dips gently towards the Horseshoe valley. This
303 surface dips approximately 1.5° , is very uneven, has a wavy appearance comprising
304 undulations that vary from hundreds of meters to more than 10 km in length, and 0.5 km
305 to 5 km across (Figs. 4 and 5).

306 The Portimão plateau is an E-W elongated surface limited by the two prominent
307 escarpments which constitute flanks of the D. Carlos and Cadiz valleys. The northern
308 escarpment is sinuous, whilst the southern one, is fairly rectilinear, trending WNW-
309 ESE, draped by recent sediments carried by the local drainage. The top of this plateau
310 shows circular positive reliefs, the larger one of which has been labeled here as the D.
311 Carlos salt diapir (Figs. 1, 4 and 6D), whose origin is discussed elsewhere in this paper.

312 **2.3. The Horseshoe Abyssal Plain**

313 The extremely flat HAP has general slopes of less than 0.1° sharply contrasting with the
314 slopes of the foot of its boundaries, between 5° and 10° in general.

315 The foot of the slope of the Gorringe Bank presents a remarkable offset of about 14 km
316 at roughly 11° W (Fig. 4). This offset lies at the end of a valley that originates at the
317 Gorringe saddle (see fig. 1 for location). It is also clear that the southern flanks of the
318 Gettysburg and Ormonde seamounts display fairly different topographic roughness. The
319 Ormonde southern flank smooth topography resembles the morphological types of the

320 continental slope or of the Sagres plateau, whilst the edges of the Gettysburg and Coral
321 Patch Ridge display a similar wrinkled surface. It is possible that this offset and valley
322 coincide with the ocean-continent boundary proposed by Rovere et al. (2004) at the
323 Gorringe Bank.

324 The interior of the HAP is only locally perturbed by four elongated groups of hills that
325 rise between 40 m and 200 m above seafloor (Fig. 4 and 6E). The largest of these
326 groups is 16 km in length and the largest individual hill is 6 km long. The hills in each
327 group are aligned along approximately E-W directions and each one of the hills has
328 their crest parallel to NE-SW, approximately. These hills are aligned along the WNW-
329 ESE oriented tectonic morphological lineaments described and discussed elsewhere in
330 this paper.

331 **2.4. Lineaments**

332 Long WNW-ESE trending discrete lineaments of tectonic origin were for the first time
333 revealed in the Gulf of Cadiz sea floor by the MATESPRO multibeam survey (Duarte et
334 al., 2005 and Rosas et al., 2009). These lineaments consist of an aligned series of
335 elongate WNW-ESE trending crests and troughs, more or less continuous, with a typical
336 width of a few hundreds of meters (Figs. 4 and 7). Pervasive sets of E-W linear
337 undulations, up to 8km long, accompany these lineaments (Fig. 7). To the east of the
338 Horseshoe escarpment these lineaments present uninterrupted segments as large as 100
339 km of length, approximately, while in the Horseshoe Abyssal Plain these lineaments are
340 discontinuous. Altogether, from the Gorringe Bank flank across the Horseshoe Abyssal
341 Plain and lower continental slope of the Gulf of Cadiz, lineaments of 250 km can be
342 identified, from approximately 4870 to 2000 mbsl (Fig. 4). It is worthwhile to note that
343 various mud volcanoes sit on top of the lineaments (Figs. 2 and 4).

344

345 **3. Structure of the NW part of the Gulf of Cadiz**

346 A structural map of the study area based on the interpretation of the MATESPRO
347 bathymetry and available MCS profiles is presented in Fig. 8. The main faults are here
348 described based on MCS profiles that are quoted from published works or presented
349 here. Fig. 8 also shows a compilation of focal mechanisms and main horizontal
350 compression taken from Ribeiro et al. (1996).

351 **3.1 WNW-ESE to E-W Faults**

352 One of the most prominent features in the north-western part of the Gulf of Cadiz is the
353 above described WNW-ESE to E-W trending set of valleys, escarpments and lineaments
354 (Figs. 4 and 7). The seismic lines that are shown in Figs. 9 to 11 and hereafter described
355 show that all these features are associated with faults, whose geometry and kinematic
356 history are different.

357 The D. Carlos and Cadiz valleys that bound the Portimão plateau sit on top on two
358 faults, as shown in Fig. 9. According to this the Portimão plateau can be interpreted as a
359 pop-up structure. The D. Carlos valley lies at the south-western edge of the
360 Guadalquivir acoustic basement high that, at the precise location of this seismic profile,
361 bears a WNW-ESE strike as can be seen on the bathymetry (Fig. 4). The drag evident in
362 the sediments of the uppermost sequence and the superficial gravity extensional faults
363 indicate that the northernmost valley flank fault is undergoing extensional deformation
364 at Present. The folds in the Mesozoic through Miocene-Lower Pliocene of the central
365 and northern parts of the Portimão pop-up depict an asymmetry that indicates
366 northwards tectonic transport on top of the acoustic basement fault.

367 Since it has been known for long that the Guadalquivir Bank is made up of Variscan
368 basement metamorphosed flysch of Carboniferous age (e.g. Ribeiro et al., 1979, Gràcia
369 et al., 2003) the stratigraphy across the northern fault of the Faro valley implies that it

370 played an extensional role during the Mesozoic followed by northwards directed
371 thrusting during the Paleogene through Miocene and resumed extensional movement
372 during Pliocene-Quaternary times.

373 The southern boundary of the Portimão pop-up block shows both the topography and
374 the Mesozoic through Quaternary sedimentary packages dipping to the south (Fig. 9).

375 The following features are also evident in the seismic line across the southern part of

376 Portimão plateau (Fig. 9), as follows: i) tectonic deformation affects the topmost

377 sediments (Fig. 6F), ii) the pre-Pliocene folds asymmetry is southwards verging, iii)

378 there is no correspondence on the seismic stratigraphy between the pre-Pliocene

379 sediments of the Portimão pop-up and the southern counterpart and iv) the Mesozoic

380 units show a wedge geometry. From these observations it is inferred that, firstly, this

381 boundary of the Portimão plateau is an old fault with opposite dip with respect to the

382 north boundary of the plateau, secondly, this was a northerly dipping extensional fault

383 during the Mesozoic, thirdly, it was inverted with a southwards directed tectonic

384 transport during the Paleogene through Miocene times and, fourthly it is going tectonic

385 deformation at Present.

386 The southernmost segment of the seismic profile in Fig. 9 cuts across the Cadiz valley

387 and up slope the gently dipping north western part of the Gulf of Cadiz accretionary

388 wedge. The profile shows a sub-horizontal, mildly deformed sequence of sediments

389 covering the chaotic seismic facies of the accretionary wedge or imbricate thrust wedge,

390 as described by Gutscher et al. (2002) and Iribarren et al. (2007), respectively. The base

391 of the chaotic seismic facies unit is made up by coherent high amplitude reflectors here

392 interpreted as Jurassic through Cretaceous syn-rift sediments on top of which detached

393 the thrust wedge. It is worthwhile to note that these sediments are disrupted by vertical

394 discontinuities, with small vertical displacement, that can be followed up into the
395 chaotic body and overlying topmost sequence.

396 The sub-vertical discontinuity that separates the Portimão plateau from the southern
397 plain is neither compatible with thrusting nor with extensional tectonics (Fig. 9).

398 Alternatively, it is interpreted as a transpressive E-W trending strike-slip fault at Present
399 based on the fact that it displays evidence of shortening structures, folds and north
400 wards and south wards directed thrusts on both sides of the fault. These observations
401 imply that the main compression direction rotated from high angle to low angle with
402 respect to the E-W strike of the faults, which is compatible with the counter-clockwise
403 rotation of the movement of Africa with respect to Iberia in the Cenozoic, from
404 approximately south to north in the Paleogene, to south east to north west in the
405 Miocene to ESE to WNW in the Present (Dewey et al., 1989).

406 The circular dome protruding the top of the Portimão plateau depicted in the bathymetry
407 is interpreted as D. Carlos salt diapir (Figs. 1, 4 and 10). The salt does not outcrop at the
408 surface but is popping-up underneath the sedimentary cover. The two reverse faults that
409 bound this structure were interpreted as smaller scale structures accommodating internal
410 shortening across the Guadalquivir Bank by Zitellini et al. (2004). This is a clear
411 example where the map view image clarifies specific not fully understood superficial
412 structures in reflection seismics.

413 The deep structure of the WNW-ESE trending lineaments (Fig. 8) is imaged in the
414 seismic profiles shown in Figs. 9,10 and 11 in the work of Rosas et al. (2008). It can be
415 seen in these seismic profiles that the rectilinear morphologic lineaments overlie vertical
416 discontinuities that are rooted far below the accretionary wedge detachment, i.e. into the
417 Jurassic sediments. These discontinuities cut the Mesozoic into blocks of 3-5 km of
418 width, with small vertical offset and stratigraphic mismatch. The symmetry of the

419 upward drag of the seismic horizons with respect to these discontinuities from the
420 deepest stratigraphic levels across the chaotic facies, the disturbance observed in the
421 cover sediments and the existence of mud volcanoes sitting on top of these lineaments
422 (Figs. 8 and 12), strongly argues in favour of upward injection of fluids along these
423 faults (cf. with Figs. 9 and 11). These characteristics strongly suggest that these
424 discontinuities can correspond to tensile fractures with a strike-slip movement
425 component.

426 The pervasive set of E-W trending undulations that accompany the E-W to WNW-ESE
427 trending faults are en echelon folds (Fig. 7 and 11), i.e. kinematic indicators that show a
428 dextral strike-slip lateral movement on these faults.

429 The growth wedge of Mesozoic sediments clearly associated to some of these WNW-
430 ESE trending faults (Fig. 10) is another indication for the deep root of these faults.

431

432 **3.2. N-S to NE-SW faults**

433 The Aljezur canyon-Sagres valley and the Portimão canyon sit on top of the offshore
434 prolongation of the Aljezur and Portimão faults, respectively (Figs. 2 and 8). Inspection
435 of the seismic profiles confirm the Pliocene –Quaternary activity of these faults that
436 show an important decrease in tectonic deformation after Miocene times (Figs. 12 and
437 13). The offshore mapping of these faults shows they have continuous segments larger
438 than 100 km in length that, when added together with the onshore segments, they
439 constitute discontinuous steep faults of approximately 200 km long, as happens with the
440 left lateral strike-slip late Variscan faults in the central and northern parts of the Iberian
441 peninsula (Ribeiro, 2002; Arthaud and Matte, 1977), which are also active in the
442 Quaternary (Cabral, 1989).

443 The Tagus Abyssal Plain Fault is proposed on the basis of the N-S trending sharp
444 morphological scarp that lies to the north of the Gorringe Bank thrust. However, recent
445 unpublished work by Cunha (2008) confirms the existence of this reverse fault that
446 cross cuts Pliocene-Quaternary sediments.

447 The São Vicente Fault strikes NE-SW (Fig. 14) outcrops along the southeast flank of
448 the São Vicente canyon. It is a southeastwards dipping steep fault, possibly part of the
449 Odemira-Ávila fault (also known as the Messejana dyke), an approximately 600 km
450 long vertical left-lateral late Variscan fault intruded by a basic dyke of Early Jurassic
451 age (Dunn et al., 1998). Pliocene-Quaternary vertical displacement along this fault
452 onshore was described by Cabral (1995).

453 The NE-SW trending Horseshoe fault was described as an active fault in the Present by
454 Gràcia et al. (2003) and Zitellini et al. (2004), has a cluster of seismicity associated to it
455 (Figs. 1 and 2). Its fault scarp is very well depicted in the MATESPRO bathymetry,
456 from the Coral Patch Ridge well into the South Portuguese continental slope bordering
457 the Sagres plateau. It can be seen that the height of the scarp increases northwards and it
458 is intercepted by WNW-ESE trending faults. At these interceptions the Horseshoe fault
459 scarp is either deflected or offset across the WNW-ESE dextral strike-slip faults and
460 landslides formed (Figs. 4, 5, 6C and 8).

461 The NE-SW escarpments at the back of the Horseshoe fault host some of the crescent
462 shaped Giant Scours described elsewhere in this work. These scarps sit on top of blind
463 thrusts, as shown in Fig. 15 that appear to be recent reactivation of individual faults
464 from within the Gulf of Cadiz Accretionary Wedge or Gulf of Cadiz Imbricate Unit,
465 after Gutscher et al (2002) or Iribarren et al. (2007), respectively. Single channel
466 seismic line across two of the Giant Scours show that the internal parts of the crescents
467 consist of depressions filled in with upslope prograding sedimentary units. These units

468 develop towards the Giant Scour crescent shaped scarp, which sharply truncates
469 sediments behind it (Fig. 16).

470 **3.3. Chaotic Seismic Units**

471 The MATESPRO bathymetry clearly shows the divide between the wrinkled
472 topography that overlies the Gulf of Cadiz Accretionary Wedge, after Gutscher et al.
473 (2002) and the surrounding smoother areas (Figs. 2 and 4). The MCS profiles shown in
474 Figs. 12 and 15 show the existence of a complex of stacked thrusts underneath the
475 wrinkled surface of the so-called accretionary wedge and also under the smoother
476 topography of the Sagres and Cadiz valleys.

477 In all seismic profiles it is evident that the complex of stacked thrusts is overlain by a
478 package of sediments that is not involved in the thrust stacking. The thickness of this
479 sedimentary cover is generally around 0.3-05 sec. TWT and the earliest age of these
480 sediments is Early Pliocene after Roque (2007). However, this sedimentary cover is
481 deformed by the E-W to WNW-ESE dextral strike-slip faults and by discrete
482 reactivation of individual thrusts of the stacked thrusts units, as described elsewhere in
483 this work, as well as, by widespread extrusion of mud volcanism, gravitational faulting
484 described by various authors as mentioned before.

485 A unit of chaotic facies that has neither coherent internal layering nor imbricate fabrics,
486 probably an olistostrome, is shown in Fig. 10. This unit is not involved in the thrust
487 stacking of the accretionary wedge and is overlain by the well layered Pliocene-
488 Quaternary sediments. This olistostrome lies between the Portimão Bank and the
489 wrinkled surface of the Gulf of Cadiz Accretionary Wedge, in the Cadiz valley. It is
490 worthwhile to note that the olistostrome pinches out on top of the Portimão Bank,
491 suggesting that it could have been fed from the uplifted area of the Portimão Bank
492 during the Tortonian phase of compression, i.e. the pop-up of the bank.

493 **4. Discussion**

494 **4.1. Morphology and tectonics**

495 **4.1.1. The escarpments and seamounts**

496 It was shown in this paper that the E-W trending Portimão Bank formed initially as a
497 graben during Mesozoic times, was subsequently inverted during the Paleogene and
498 Miocene compression and is now, probably since Early Pliocene times, undergoing
499 dextral transpressive strike-slip deformation along its southern boundary, whilst the
500 northern boundary experiences local extension due to a releasing bend formed by the
501 basement fault. Seismicity and focal mechanisms (Fig. 2) attest for the compression at
502 the southern edge of this seamount, preferentially concentrated to the east of the study
503 area where the fault becomes NE-SW trending, i.e. at a higher angle to the main NW-SE
504 oriented compression direction.

505 The Sagres plateau is bound by the NE-SW trending Horseshoe thrust of Miocene age
506 in the west (Gràcia et al., 2003, Zitellini et al., 2004) and the steeply dipping Aljezur
507 fault in the east. The height of the plateau diminishes towards the south and its
508 morphological expression disappears at the contact with one of the WNW-ESE strike-
509 slip faults. The cluster of instrumental seismicity in Fig. 2 attests for its present day
510 activity (Stich et al., 2007).

511 The Marquês de Pombal plateau also resulted from tectonic inversion of an N-S
512 trending continent-wards directed extensional fault. The Pereira de Sousa fault is a N-S
513 trending steep Mesozoic rift fault still in activity at Present (Gràcia et al., 2003; Terrinha
514 et al., 2003).

515 The north westwards directed Gorringe Bank thrust with a paroxysmal activity in the
516 Tortonian (after Tortella et al. 1997; Sartori et al., 1994) is still an active structure as
517 attested by the instrumental seismicity cluster (Fig. 2).

518 It can be concluded that the escarpments, seamounts and uplifted plateaus of the study
519 area, all formed in association with compressive tectonic events and resulted from
520 polyphase tectonics. The Pereira de Sousa fault escarpment is the only one that owes its
521 morphology mostly to the Mesozoic rifting.

522 The tectonic shaping processes are still active in the Present, as shown by the on-going
523 formation of very recent features that are indicative of uplift and tectonic instability,
524 such as the popping-up of the D. Carlos salt diapir (Fig. 10), the mass wasting
525 processes, such as submarine slides and various manifestations of soft sediment
526 deformation and mass wasting processes in the Sagres plateau-Aljezur canyon, the São
527 Vicente canyon and the Portimão plateau, Horseshoe Faul scarp, as well as, on the
528 Marquês de Pombal, Gorringe and Pereira de Sousa escarpments as described by Gràcia
529 et al.(2003), Terrinha et al.(2003) and Vizcaíno et al.(2006).

530 **4.1.2. The Giant Scours**

531 The Giant Scours are crescent-shaped depressions with scarps that can reach more than
532 100 meter in high and slopes up to 27° located in a relative flat area of the Horseshoe
533 Valley that collects the sediments from the Northern and North-eastern parts of the Gulf
534 of Cadiz (Figs. 4, 5 and 7). The scours sit on the edge of folds draping Pliocene to
535 Quaternary thrusting and the frontal depressions are filed up with upslope
536 progradational bodies (Figs. 15 and 16). These bodies can be interpreted as been fed by
537 material withdrawn from the retreating scarps (Fig. 17; Duarte et al., 2007). This
538 scenario requires the existence of continuous scouring and sedimentation at unusual
539 depths by means of bottom currents, possibly of turbidite origin as documented offshore

540 the Shetland Islands and Monterrey East Channel (Kenyon et al., 2000; Kenyon et al.,
541 2006; Fildani et al., 2006). The interaction of bottom and turbidity currents with
542 seafloor morphological features formed by Recent tectonic activity can lead to flux
543 separation and formation of vortexes that cause seafloor erosion and the formation of
544 scours. These processes were proposed for the formation of similar structures in other
545 places and different geological settings between 600m and 3500m water depth
546 (Faugères et al., 1997; Bulat and Long, 2001; Verdicchio and Trincardi, 2006; Fildani et
547 al., 2006). This process could account simultaneously for the formation of the scarp of
548 the scour, the progradational bodies and the maintenance of the scarp, at least as long as
549 the bottom current lasted and the retreating escarpment does not meet an obstacle.
550 An alternative model is that the Giant Scours could form due to the interaction of along
551 slope bottom currents with the sea floor, such as the North Atlantic Deep Water. This
552 interaction could lead to the formation of giant eddies that could locally erode and
553 amplify pre-existing tectonic escarpments. However, the existence of along slope
554 currents at these depths has not been documented in this area.
555 Evidences for alternative mechanisms for the formation of these features, such as slide-
556 slump processes caused by slope instabilities or collapse processes associated with fluid
557 escape along major tectonic structures (similar to those of pockmark formation), were
558 not observed on the present dataset despite the evidences for mass wasting processes,
559 and the existence of widespread mud volcanism and fluid migration activity in other
560 areas of the Gulf of Cadiz.

561

562 **4.1.3. The canyons**

563 The São Vicente and Portimão canyons are by far the deepest incisions on the northern
564 margin of the Gulf of Cadiz and they are underlain and controlled by important steep

565 faults. The Aljezur canyon-Sagres valley system is also controlled by a steep fault.
566 These offshore faults connect with other that were inherited from the late Variscan
567 fracturing, subsequently re-activated during the Mesozoic rifting and Cenozoic tectonic
568 inversion (see Fig. 2).

569 The MCS profiles shown in this work attest for the Quaternary activity of these faults
570 but also show that the deformation after Miocene times has severely diminished in the
571 case of the Portimão and Aljezur faults.

572 Gràcia et al. (2003) and Zitellini et al. (2004) showed the important activity of the
573 northern segment of the Horseshoe fault that constitutes the eastern flank of the terminal
574 part of the São Vicente canyon.

575 The São Vicente and Portimão canyons show important gravity slides on their western
576 flanks. This can be interpreted as caused by the increase of the tilting associated with
577 the west wards directed thrusting of the Marquês de Pombal and Horseshoe faults.

578 Alternatively, in the Sagres valley the sliding can be caused by excavation at the
579 meeting point of this valley with the Cadiz valley.

580 The minor present day tectonic deformation on the faults that control the localization of
581 the canyons together with the important incision and land sliding close to the active
582 Marquês de Pombal and Horseshoe thrusts can be interpreted as an indication of passive
583 uplift of the continental slope carried on top of these thrusts.

584 **4.1.4. The chaotic bodies**

585 Three bodies of chaotic facies were distinguished in this work, all covered by a unit
586 hemipelagic sediments usually of 0.3 – 0.5 sec TWT. One is referred to as the Gulf of
587 Cadiz Accretionary Wedge (GCAW) by Gutscher et al. (2002) or alternatively as the

588 Gulf of Cadiz Imbricate Wedge by Iribarren et al. (2007). This body has a strong
589 morphologic imprint on the seafloor morphology (Fig. 12).

590 A second one, that extends across the Horseshoe Abyssal Plain and Horseshoe Valley,
591 has been considered as a gravitational unit, an olistostrome (e.g. Torelli et al., 1997;
592 Iribarren et al., 2007). It is shown in this paper that this unit (Figs.12 and 15) has
593 imbricate seismic reflections that are interpreted as stacked thrusts, some of which have
594 been recently reactivated forming blind thrusts morphologic scarps where the Giant
595 Scours nucleated. These recent scarps are, however, the only morphologic manifestation
596 on the seafloor surface of this body.

597 A third body with internal non-organized chaotic facies overlies the first described one,
598 as shown in Fig. 10.

599 It is shown in this work that the two first described bodies consist of complexes of
600 stacked thrusts and that the GCAW overthrusts the second one to the west (Fig. 10).
601 Considering that these are tectono-stratigraphic units we speculate that only one
602 accretionary wedge (or imbricate wedge) formed during the latest Cretaceous and
603 Paleogene (perhaps through the Early Miocene). This event occurred before the
604 Gibraltar arc formed (when the Internal Betic terranes were still a long way farther east,
605 Fig. 18B). Then, from Early Miocene to earliest Pliocene (or Messinian?) times, when
606 the Gibraltar orogenic arc formed, a part of this accretionary wedge was tectonically
607 reworked forming the present day GCAW and its wrinkled topography (Fig. 18C).
608 From the Pliocene to Present the thrust stacking within the GCAW severely diminished
609 and the WNW-ESE dextral strike-slip faults formed (Fig. 18 d).

610 From a genetic point of view we consider the first two chaotic bodies as tectonic
611 melanges made up of tectonised olistostromes and tectonosomes (see Camerlenghi and
612 Pini, 2009 for discussion). The third chaotic body is a non tectonised olistostrome.

613 **4.1.5. The WNW-ESE lineaments, strike-slip faults and recent folding**

614 The WNW-ESE lineaments shown by the MATESPRO bathymetry in this paper (Fig.
615 7) display a series of en echelon folds materialized on the most recent seafloor soft
616 sediments that indicate strain accumulation by means of dextral strike-slip (Fig. 3 and
617 6). Rosas et al. (2008) using quantitative strain analysis, analogue modelling and MCS
618 data showed that these en echelon folds result from Quaternary reactivation of basement
619 faults.

620 Inspection of MCS profiles in this paper show that these WNW-ESE faults are deeply
621 rooted into the Jurassic –Cretaceous rift sequences, which is compatible to observations
622 made onshore in the Algarve Basin at the Lower Jurassic of the S. Vicente cape (Ribeiro
623 and Terrinha, 2007).

624 These faults also serve as conduits for the exhalation of fluidized sediments that form
625 some of the Gulf of Cadiz mud volcanoes (Fig. 2), which is another evidence of the
626 recent activity of the faults and also that they cut through the Gulf of Cadiz accretionary
627 prism. Moreover, as shown on the MCS profile in Figs. 11 and 12, these strike-slip
628 faults allow the escape of fluids from within deep in the Mesozoic sequences, probably
629 at the Hettangian stratigraphic level that hosts the salt in south Portugal and northwest
630 Morocco (Terrinha, 1998).

631 The strike-slip faults and folding are also active in the Horseshoe Abyssal Plain.
632 However, the scarce morphotectonic features associated to these faults in the Horseshoe
633 Abyssal Plain when compared to the continental slope to the east, suggests a westwards

634 propagation of the recent deformation on the WNW-ESE faults, away from the
635 Gibraltar Arc.

636 Because i) these faults have only recently been reactivated as strike-slip faults, ii) they
637 strike at only a small angle to the present day trajectory of Africa with respect to Iberia,
638 according to recently reported geodetic models (Fig. 8), iii) their minimum length
639 exceeds 230 km as shown in the presented bathymetry and iv) they cut across the
640 Horseshoe Abyssal Plain and the Gulf of Cadiz accretionary wedge; it is here suggested
641 that they will play an important tectonic role in the new tectonic framework that is
642 presently under development between Iberia and Nubia. As a matter of fact, some of the
643 WNW-ESE faults described here are located within a 600 km x 40 km shear zone
644 proposed by Zitellini et al. (2009) as a segment of the Eurasia-Nubia plate boundary that
645 spans from the eastern tip of the Gloria Fault to the Rif-Tell plate boundary in north-
646 western Morocco (Morel and Meghraoui, 1996).

647 **4.2. Strain partitioning, deformation migration and seismicity**

648 The studied dataset shows that the E-W trending faults were inherited from the Jurassic-
649 Lower Cretaceous rifting and subsequently inverted as reverse faults during the
650 Cenozoic (Fig. 8); the same applies to the NE-SW to N-S trending faults as shown in
651 previous works (Terrinha, 1998; Rovere, 2004; Terrinha et al., 2002; Terrinha et al.,
652 2003; Gràcia et al., 2003a; Ribeiro and Terrinha, 2007). It was also shown that the Gulf
653 of Cadiz accretionary wedge has diminished significantly its activity since latest
654 Miocene times, possibly Early Pliocene, although disperse thrusts that still remain blind
655 underneath the Messinian-Recent sediments are presently reactivated (Fig. 12 and 15).
656 Based on the presented dataset, we propose that the present day WNW-ESE convergent
657 movement of Africa with respect to Iberia generates deformation in the study area,

658 which is accommodated through partitioning on two approximately orthogonal fault
659 sets, as follows. An N-S to NE-SW striking set of faults that accommodate shortening
660 mainly by thrusting and an E-W to WNW-ESE striking, generally sub-vertical, set of
661 faults that accommodate dextral strike-slip faulting.

662 The first set comprehend the main thrust faults of the area, Horseshoe Fault, Marquês de
663 Pombal fault and Tagus Abyssal Plain fault (see map of Fig. 2) that extend the Present
664 east to west shortening for approximately 300 km from the South, near the contact with
665 the Coral Patch Ridge (35.5°N), towards the north, along the West Portuguese Margin
666 until a latitude of 38°N, as recently shown by Neves et al. (2008).

667 The second fault set is deeply rooted in Jurassic through Cretaceous rifting faults and
668 were reactivated mainly in the Pliocene-Quaternary as dextral strike-slip faults, which is
669 compatible with the present day movement of Nubia with respect to Iberia. These faults
670 show considerably higher degree of deformation in the east than in the west, which
671 argues in favour of propagation of deformation from east to west.

672 The thrusting on the N-S Marquês de Pombal fault is recent, as well as, on the Gorringe
673 Bank fault (that had a quiescence period after the Tortonian), on the Tagus Abyssal
674 Plain Fault (Cunha, 2008) and at the N-S trending faults at 38°N (Neves et al., 2008).

675 Altogether, these observations lead us to argue that the deformation is migrating from
676 the realm of Gibraltar to the west and along the Portuguese West Margin to the north.

677 Considering the sub-parallel strike of the N-S to NE-SW faults, their common origin in
678 the Permian and reactivation during the Mesozoic rifting and Cenozoic inversion, it is
679 here suggested that this 300 km en-échelon fault zone can have a common detachment,
680 underneath SW Iberia. Since the tomography data presented in Gutscher et al. (2002)
681 suggests that the Horseshoe may penetrate at least till 100 km in the lithosphere, the 300

682 km long N-S trending fault system should be considered as *firstly*, a possible source
683 candidate for the Lisbon 1/11/1755 earthquake and *secondly*, the propagation of a new
684 front of compressive deformation towards the north along the West Portuguese Margin,
685 which will eventually lead to the nucleation of a West Iberia incipient subduction zone,
686 as proposed by Ribeiro et al. (1996).

687 Alternatively, even if these faults do not have a common detachment, a complex
688 rupture scenario can be envisaged to explain the large energy released during the 1755
689 event. Complex seismic ruptures have been documented in other locations, such as, for
690 instance the 1958 Gobi-Altay event which produced 260 km of surface rupture from the
691 segmented main fault with a strike-slip movement and simultaneous rupture of nearby
692 thrust faults (Kurushin et al., 1997), or the Tangshan earthquake of 1976, which was a
693 combination of several ruptures, strike-slip and thrust faults, following each other only a
694 few tens of seconds (Butler et al., 1979). The hypothesis of complex ruptures involving
695 triggering or “domino-effect” is consistent with the majority of the historical documents
696 that report a very long vibration (up to 20-30 minutes) and various sub-events for the 1st
697 November 1755 earthquake (e.g. Martinez Solares, 2001).

698 We also speculate that the location of recent epicentres in front of the Horseshoe fault in
699 the Horseshoe Abyssal Plain, such as the 1969 event ($M_s=7.9$) (Fukao, 1973), as well as
700 the $M_w=6.0$ 12/02/2007 and the $M_L=4.5$ 21/06/2006 events (Stich et al., 2007), all with
701 an major dip-slip component can be interpreted as an indication of nucleation of new
702 thrusts to the west of the main Horseshoe fault.

703 The NW-SE S_{Hmax} direction calculated from earthquake focal mechanism is in very
704 good agreement with the Eurasia-Africa convergence direction estimated by the
705 NUVEL-1 model (DeMets et al., 1994). However, recent estimates of this velocity
706 using space geodetic techniques, and considering the Africa plate split into Nubia and

707 Somalia, give for the Nubia-Eurasia collision a WNW-ESE direction, in the middle of
708 the Gulf of Cadiz (Fig.8). This discrepancy is interpreted as the coupled result of strain
709 partitioning on E-W and NNE-SSW trending faults and aseismic deformation along the
710 plate boundary.

711 **5. Conclusions**

712 The following conclusions are withdrawn.

- 713 1. The escarpments, seamounts and uplifted plateaus of the study area, all formed in
714 association with polyphase compressive tectonic events from the late Cretaceous
715 through Present, with the exception of the Pereira de Sousa fault escarpment that owes
716 most of its morphology to the Mesozoic rifting. The Quaternary uplift has generated
717 mass transport deposits (also reported by Gràcia et al. (2003), Terrinha et al. (2003) and
718 Vizcaíno et al. (2006)), kilometric scale soft sediment unstable folds on the continental
719 slope and incision of the canyons.
- 720 2. The Giant Scours display erosive and depositional structures that result from vortexes
721 of high-density bottom currents at the edge of scarps formed at the crest of blind thrusts
722 anticlines of Recent age.
- 723 3. The chaotic bodies buried under uppermost Miocene – lower Pliocene sediments in
724 the Horseshoe Abyssal Plain and Horseshoe Valley together with the GCAW formed as
725 stacked thrusts (possibly an accretionary wedge) in the Late Cretaceous-Earliest
726 Miocene times before the emplacement of the Gibraltar orogenic Arc. Miocene
727 reactivation of the eastern part of this body originated the GCAW and thrusting of this
728 tectono-stratigraphic unit to the west. The third chaotic body corresponds to a non
729 tectonised olistostrome that seals the most important thrust stacking in early Pliocene
730 times.

731 4. The WNW-ESE trending lineaments are the superficial expression of steep faults
732 deeply rooted in the Mesozoic substratum and underlying acoustic basement or
733 Paleozoic basement onshore. Segments of these faults acted as rift faults during the
734 Mesozoic and were reactivated in Quaternary times as strike-slip faults that cross cut the
735 NE-SW trending thrusts.

736 5. The present day NW-wards movement of Nubia with respect to Iberia generates
737 strain partitioning by means of dextral wrenching on WNW-ESE trending steep faults
738 and thrusting on the NE-SW trending fault in the Gulf of Cadiz and Horseshoe Abyssal
739 Plain. Further north, at the base of the continental slope of the southernmost part of the
740 West Iberia Margin, NNE-SSW to N-S westerly dipping thrusts accommodate
741 shortening in an area where wrenching has not been observed, which indicates that
742 westward directed thrusting propagated from the Gibraltar Arc to the west (Horseshoe
743 Fault) and to the north along the Portuguese margin (Marquês de Pombal Fault and
744 Tagus Abyssal Plain Fault).

745

746 **Acknowledgments**

747 The work was sponsored by MATEPRO (PDCTM/P/MAR/15264/1999),
748 EUROMARGINS SWIM (01-LEC-EMA09F), MVSEIS (01-LEC_EMA24F; PDCTM
749 72003/DIV/40018) and TOPOMED (TOPOEUROPE/0001/2007) projects . Instituto
750 Scienze Marine (CNR) Bologna contribution 1587. JD and VV benefited from PhD
751 grants from Fundação para a Ciência e a Tecnologia (SFRH/BD/31188/2006,
752 SFRH/BD/17603/2004). We acknowledge the PARSIFAL Project MAR1998-1837-CE
753 for the use of bathymetry data. We also wish to thank to the captain Cte. Paulo
754 Marreiros and his crew of the NRP D. Carlos I. We acknowledge the financial support
755 from the ESF EuroMargins Program,

756 contract n. 01-LEC-EMA09F and from EU Specific Programme “Integrating
757 and Strengthening the European Research Area”, Sub-Priority 1.1.6.3,
758 “Global Change and Ecosystems”, contract n. 037110 (NEAREST). We acknowledge
759 the support by Landmark Graphics Corporation via the Landmark University Grant
760 Program.

761

762 **References**

763

764 Ambar, I., Serra, N., Brogueira, M.J., Cabecadas, G., Abrantes, F., Freitas, P.,
765 Gonçalves, C., Gonzalez, N., 2002. Physical, chemical and sedimentological aspects of
766 the Mediterranean outflow off Iberia. *Deep-Sea Research Part II-Topical Studies in*
767 *Oceanography*, 49, 4163-4177.

768

769 Argus, D.F., Gordon, R.G., DeMets, C., Stein, S., 1989. Closure of the Africa-Eurasia-
770 North America plate motion circuit and tectonics of the Gloria fault. *Journal of*
771 *Geophysical Research*, 94,(B5), 5585-5602.

772

773 Arthaud ,F., Matte, P., 1977. Late Paleozoic strike-slip faulting in Southern Europe and
774 Northern Africa: result of a right-lateral shear zone between the Appalachians and the
775 Urals, *Geological Society of America Bulletin*, 88, pp. 1305-1320.

776

777 Banda, E., Torné, M., IAM group, 1995. IAM group investigates deep structure of
778 ocean margins. *EOS (transaction of Am. Gephys. Union*, v.76, pp. 25-29.

779

- 780 Baptista, M.A., Miranda, J.M., Chierici, F., Zitellin, N., 2003. New study of the 1755
781 earthquake source based on multi-channel seismic survey data and tsunami modeling.
782 *Natural Hazards and Earth System Sciences* 3: 333-340.
783
- 784 Baptista, M.A., Miranda, P.M.A., Miranda, J.M., Victor, L.M., 1998. Constrains on the
785 source of the 1755 Lisbon tsunami inferred from numerical modelling of historical data
786 on the source of the 1755 Lisbon tsunami. *Journal of Geodynamics* 25(1-2): 159-174.
787
- 788 Bulat J., Long D., 2001. Images of the seabed in the Faroe-Shetland Channel from
789 commercial 3D seismic data. *Marine Geophysical Researches* 22, 345–367.
790
- 791 Butler, R., Stewart, G.S., Kanamori, H., 1979. The July 27, 1976 Tangshan, China
792 earthquake-A complex sequence of intraplate events. *Bulletin of the Seismological*
793 *Society of America* 69(1): 207-220.
794
- 795 Calais, E., DeMets, C., Nocquet J.-M., 2003. Evidence for a post-3.16-Ma change in
796 Nubia-Eurasia-North America plate motions? *Earth and Planetary Science Letters*,(216),
797 81-92.
798
- 799 Calais, E., Nocquet, J.-M., Jouanne, F., Tardy, M., 2002. Current strain regime in the
800 Western Alps from continuous Global Positioning System measurements, 1996-2001.
801 *Geology* 30(7): 651-654.
802

- 803 Calais, E., Nocquet, J.-M., Jouanne, F., Tardy, M., 2002. Current strain regime in the
804 Western Alps from continuous Global Positioning System measurements, 1996-2001.
805 *Geology*, 30,(7), 651-654.
806
- 807 Cabral, J., 1989. Na example of intraplate neotectonic activity, Vilarica Basin,
808 Northeast Portugal. *Tectonics*, 8, 2, 285-303.
809
- 810 Cabral, J., 1995. Neotectónica em Portugal Continental. *Memórias do Instituto*
811 *Geológico e Mineiro*, Meméria 31, Lisboa, pp. 241.
812
- 813 Camerlenghi, A., Pini, G.A., 2009. Mud volcanoes, olistostromes and Argille scagliose
814 in the Mediterranean region. *Sedimentology*, 56, 1, pp. 319-365
815
- 816 Carrilho, F., Teves-Costa, P., Morais, I., Pagarete, J., Dias, R., 2004. GEOALGAR
817 Project: First Results on Seismicity and Fault-plane Solutions. *Pure and Applied*
818 *Geophysics* 161(3): 589-606.
819
- 820 Cunha, T., 2008. Gravity Anomalies, Flexure and the Thermo-Mechanical Evolution of
821 the West Iberia Margin and its Conjugate of Newfoundland.; PhD Thesis, Department
822 of Earth Sciences, University of Oxford.
823
- 824 DeMets, C., Gordon, R.G., Argus, D.F., Stein, S., 1994. Effect of recent revisions to the
825 geomagnetic reversal time scale on estimates of current plate motions. *Geophysical*
826 *Research Letters*, 21,(20), 2191-2194.
827

- 828 Dewey, J.F., Helman, M.L., Turco, E., Hutton, D.H., Knott, S.D., 1989. Kinematics of
829 the Western Mediterranean, in: Coward, M.P., Dietrich, D., Park, R.G (eds), *Alpine*
830 *Tectonics*, Geol. Soc. Spec. Publ. No. 45, pp. 265-283.
831
- 832 Dias, R.P., 2001. Neotectónica da região do Algarve. Dissertação de doutoramento,
833 Universidade de Lisboa, 369pp.
834
- 835 Dias, R.P., Cabral, J., 2002. Interpretation of recent structures in an area of cryptokarst
836 evolution-neotectonic versus subsidence genesis. *Geodinamica Acta*, 15 (4), 233-248.
837
- 838 Duarte, J.C., Rosas, F., Pinheiro, L.M., Matias, L.M., Carvalho, A.M, Terrinha, P.,
839 Ivanov, M., 2005. Interpretation of recent sedimentary and tectonic structures off SW
840 Iberia from multibeam bathymetry, seismic reflection and experimental modeling.
841 *Geophysical Research Abstracts*, Vol. 7, 07867.
842
- 843 Duarte, J.C., Rosas, F., Terrinha, P., Valadares, V., Taborda, R., Matias, L., Roque, C.,
844 Magalhães, V., Henriët, J.P., Pinheiro, L., 2007. Deep Submarine Giant Scours in
845 northern Gulf of Cadiz (offshore SW Iberia): a singular case of sedimentary and
846 tectonic coupling. *Geophysical Research Abstracts*, Vol. 9, 03940.
847
- 848 Dunn, A.M., Reynolds, P.H., Clarke, D.B., Ugidos, J.M., 1998. A comparison of the
849 age and composition of the Shelburne dyke, Nova Scotia, and the Messejana Dyke,
850 Spain. *Can. J. Earth Sci.* 35(10): 1110-1115.
851

- 852 Faccenna, C., Piromallo, C., Crespo-Blanc, A., Jolivet, L., Rossetti, F., 2004. Lateral
853 slab deformation and the origin of the western Mediterranean arcs. *Tectonics*
854 23(TC1012).
- 855
- 856 Faugères J.C, Gonthier, È., Bobier, C., Griboulard, R., 1997. Tectonic control on
857 sedimentary processes in the southern termination of the Barbados Prism. *Marine*
858 *Geology* 140, 117-140.
- 859
- 860 Fernandes, R.M. S., Ambrosius, B.A. C., Noomen, R., Bastos, L., Wortel, M.J.R.,
861 Spakman, W., Govers, R., 2003. The relative motion between Africa and Eurasia as
862 derived from ITRF2000 and GPS data. *Geophysical Research Letters*, 30,(16).
- 863
- 864 Fildani, A., Normark, W.R., Kostic, S., Parker, G., 2006. Channel formation by flow
865 stripping: large-scale scour features along the Monterey East Channel and their relation
866 to sediment waves. *Sedimentology* 53, 1265–1287.
- 867
- 868 Fukao, Y., 1973. Thrust faulting at a lithospheric plate boundary, The Portugal
869 earthquake of 1969. *Earth and Planetary Science Letters* 18: 205-216.
- 870
- 871 González A., Córdoba, D., Vegas R., Matias, L. M., 1998. Seismic crustal structure in
872 the southwest of the Iberian Peninsula and the Gulf of Cadiz. *Tectonophysics* 296, pp.
873 317–331.
- 874

- 875 Gràcia, E., Dañobeitia, J., Vergés, J., Bartolomé, R., 2003a. Crustal architecture and
876 tectonic evolution of the Gulf of Cadiz (SW Iberian margin) at the convergence of the
877 Eurasian and African plates. *Tectonics*, 22,(4).
878
- 879 Gràcia, E., Danobeitia, J., Vergés, J., Cordoba, D., PARSIFAL Team, 2003. Mapping
880 active faults offshore Portugal (36°N–38°N): implications seismic hazard assessment
881 along the southwest Iberian margin. *Geology*, 31,(1), 83-86.
882
- 883 Gutscher, M-A, Dominguez, S., Westbrook, G. K., Gente, P., Babonneau, N., Mulder,
884 T., Gonthier, E., Bartolome, R., Luis, J., Rosas, F., Terrinha, P., The Delila and DelSis
885 Scientific Teams, 2008. Tectonic shortening and gravitational spreading in the Gulf of
886 Cadiz accretionary wedge: Observations from multi-beam bathymetry and seismic
887 profiling, *Marine and Petroleum Geology* 26: 647-659.
888
- 889 Gutscher, M. A., Malod, J., Rehault, J.-P., Contrucci, I., Klingelhoefer, F., Mendes-
890 Victor, L., Spakman, W., 2002. Evidence for active subduction beneath Gibraltar.
891 *Geology*, 30,(12), 1071-1074.
892
- 893 Hernandez-Molina, J., Llave, E., Somoza, L., Fernandez-Puga, M.C., Maestro, A.,
894 Leon, R., Medialdea, T., Barnolas, A., Garcia, M., del Rio, V.D., Fernandez-Salas,
895 L.M., Vazquez, J.T., Lobo, F., Dias, J.M.A., Rodero, J., Gardner, J., 2003. Looking for
896 clues to paleoceanographic imprints: A diagnosis of the Gulf of Cadiz contourite
897 depositional systems. *Geology*, 31,(1), 19-22.
898

- 899 Hernández-Molina, F.J., Llave, E., Stow, D.A.V., García, M. Somoza, L., Vázquez,
900 J.T., Lobo, F.J., Maestro, A., Díaz del Río, V., León, R. Medialdea, T., Gardner, J.,
901 2006. The contourite depositional system of the Gulf of Cádiz: A sedimentary model
902 related to the bottom current activity of the Mediterranean outflow water and its
903 interaction with the continental margin. *Deep-Sea Research II* 53, 1420–1463.
904
- 905 IOC, IHO and BODC, 2003. “Centenary edition of the GEBCO Digital Atlas“,
906 published on CDROM on behalf of the Intergovernmental Oceanographic Commission
907 and the International Hydrographic Organization as part of the General Bathymetric
908 Chart of the Oceans; British Oceanographic Data Centre, Liverpool.
909
- 910 Iribarren, L., Vergés, J., Camurri, F., Fullea, J., Fernández, M., 2007. The structure of
911 the Atlantic-Mediterranean transition zone from the Alboran Sea to the Horseshoe
912 Abyssal Plain (Iberia–Africa plate boundary). *Marine Geology*, 243, 97-119.
913
- 914 Kenyon, N.H., Ivanov, M., Akhmetzhanov, A., Koslova, E.V., 2006. Interdisciplinary
915 geoscience studies of the Gulf of Cadiz and Western Mediterranean basins.
916 Intergovernmental Oceanographic Commission, Technical Series 70, UNESCO, 115 pp.
917
- 918 Kenyon, N.H., Ivanov, M.K., Akhmetzanov, A., Akhmanov, G. G., 2000.
919 Multidisciplinary Study of Geological Processes on the North East Atlantic and Western
920 Mediterranean Margins. IOC Technical Series, 56, UNESCO, 119 pp.
921
- 922 Kreemer, C., Holt, W.E., 2001. A no-net-rotation model of present-day surface motions.
923 *Geophysical Research Letters*, 28,(23), 4407-4410.

- 924
- 925 Kurushin, R.A., Bayasgalan, A., Olziybat, M., Enhtuvshin, B., Molnar, P., Bayarsayhan,
926 C., Hudnut, K.W., Lin, J., 1997. The surface rupture of the 1957 Gobi-Altay, Mongolia,
927 Earthquake. Boulder, Geological Society of America.
- 928
- 929 Lopes, F.-C., Cunha, P.P., Le Gall, B., 2006. Cenozoic seismic stratigraphy and tectonic
930 evolution of the Algarve Margin (offshore Portugal, southwestern Iberian Peninsula).
931 Marine Geology 231, 1-36.
- 932
- 933 Maldonado, A., Somoza, L., Pallares, L., 1999. The Betic orogen and the Iberian-
934 African boundary in the Gulf of Cadiz: geological evolution (central North Atlantic).
935 Marine Geology, 155,(1-2), 9-43.
- 936
- 937 Martinez-Solares, J.M., 2001. Los efectos en España del terremoto de Lisboa, Instituto
938 Geografico Nacional, Madrid, 756p.
- 939
- 940 Matias, H.C.R.C., 2007. Hydrocarbon potential of the offshore Algarve Basin.
941 Dissertação de doutoramento, Universidade de Lisboa, 324pp.
- 942
- 943 Medialdea, T., Vegas, R., Somoza, L., Vazquez ,J.T., Maldonado, A., Diaz-del Rio, V.,
944 Maestro, A., Cordoba, D., Fernandes-Puga, M.C., 2004. Structure and evolution of the
945 "Olistostrome" complex of the Gibraltar Arc in the Gulf of Cádiz (eastern Central
946 Atlantic): evidence from two long seismic cross-sections. Marine Geology, 209,(1-4),
947 173-198.
- 948

- 949 Medialdea, T., 2007. Estructura y evolucion tectonica del Golfo de Cadiz. Publicaciones
950 del Instituto Geologico y Minero de España- Serie Tesis Doctorales N°8. ISBN 978-84-
951 7840-728-2.
- 952
- 953 Morel., J.L., Megrhraoui, M., 1996. Gorringe-Alboran-Tell tectonic zone: A
954 transpressiva system along the Africa-Eurasia plate boundary. *Geology*, 24, (8), 755-
955 758.
- 956
- 957 Mulder, T., Voisset, M., Lecroart, P., Drezen, E.L., Gonthier, E., Hanquiez, V.,
958 Faugères, J.-C., Habgood, E., Hernandez-Molina, F.J., Estrada, F., Llave-Barranco, E.,
959 Poirier, D., Gorini, C., Fuchey, Y., Voelker, A., Freitas, P., Sanchez, F.L., Fernandez,
960 L.M., Kenyon, N.H., Morel, J., 2003. The Gulf of Cadiz: an unstable giant contouritic
961 levee. *Geo-Marine Letters*, V23,(1), 7-18.
- 962
- 963 Neves, M.C., Terrinha, P., Afilhado, A., Moulin, M., Matias, L., Rosas, F., 2009.
964 Response of a multi-domain continental margin to compression: study from seismic
965 reflection - refraction and numerical modelling in the Tagus Abyssal Plain.
966 *Tectonophysics*, 468, 113-130.
- 967
- 968 Niemann, H., Duarte, J., Hensen, C., Omoregie, E., Magalhaes, V.H., Elvert, M.,
969 Pinheiro, L.M., Kopf, A., Boetius, A., 2006. Microbial methane turnover at mud
970 volcanoes of the Gulf of Cadiz. *Geochimica et Cosmochimica Acta*, 70,(21), 5336-
971 5355.
- 972

- 973 Nocquet, J.M., Calais, E., 2004. Geodetic Measurements of Crustal Deformation in the
974 Western Mediterranean and Europe. *Pure and Applied Geophysics*, 161, 661-681.
975
- 976 Pinheiro, L.M., Ivanov, M.K., Sautkin, A., Akhmanov, G., Magalhaes, V.H.,
977 Volkonskaya, A., Monteiro, J.H., Somoza, L., Gardner, J., Hamouni, N., Cunha, M.R.,
978 2003. Mud volcanism in the Gulf of Cadiz: results from the TTR-10 cruise. *Marine*
979 *Geology*,(195), 131-151.
980
- 981 Pinheiro, L.M., Ivanov, M., Kenyon, N., Magalhães, V., Somoza, L., Gardner, J., Kopf,
982 A., Van Rensbergen, P., Monteiro, J.H., Euromargins MVSEIS Team, 2006a. Structural
983 control of mud volcanism and hydrocarbon-rich gas seepage: results from the TTR-15
984 and other previous cruises. *Fluid Seepages / Mud volcanism in the Mediterranean and*
985 *Adjacent Domains. CIESM Workshop Monographs*, 29, 53-58.
986
- 987 Pinheiro, L. M., Wilson, R., Pena dos Reis, R., Whitmarsh, R. B., Ribeiro, A., 1996.
988 The Western Iberia Margin: a Geophysical and Geological Overview. *Proceedings of*
989 *the Ocean Drilling Program, Scientific Results*. Whitmarsh, R. B., Sawyer, D. S., Klaus,
990 A. and Masson, D. G., College Station, TX (Ocean Drilling Program). 149: 3-23.
991
- 992 Ribeiro, A., 2002. *Soft plate and impact tectonics*, 324pp., Springer-Verlag.
993
- 994 Ribeiro, C., Terrinha, P., 2007. Formation, deformation and chertification of systematic
995 clastic dykes in a differentially lithified carbonate multilayer. SW Iberia,
996 Algarve Basin, Lower Jurassic. *Sedimentary Geology*, 196, 1-4, 2001-2015.
997

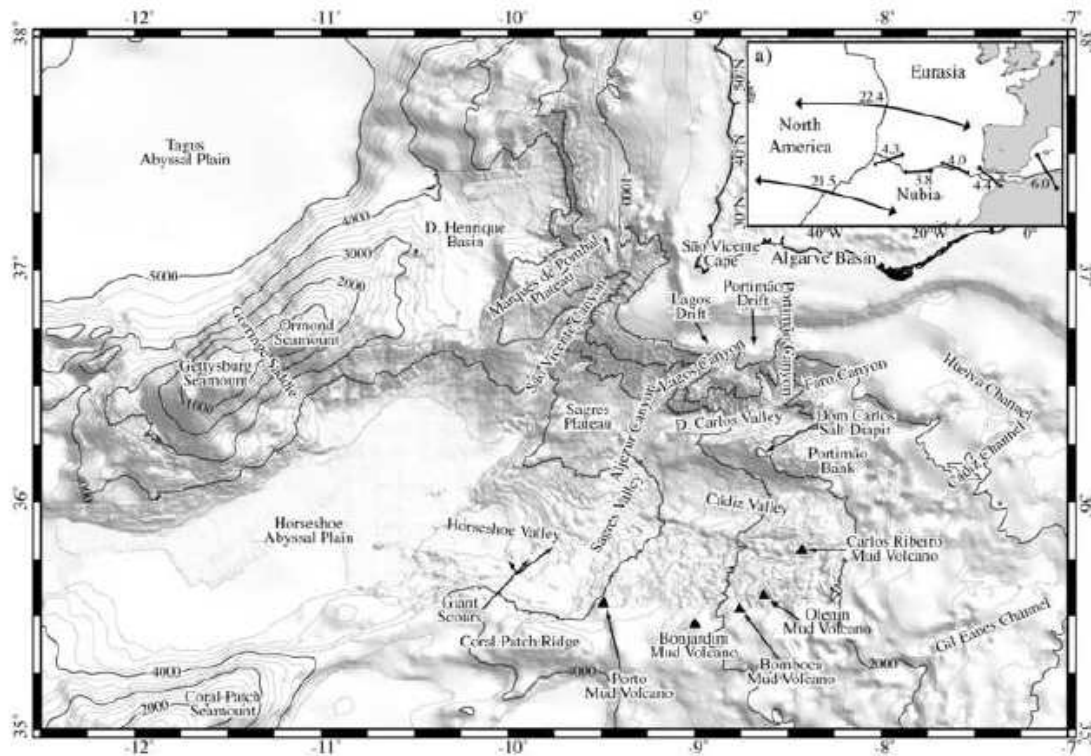
- 998 Ribeiro, A., Antunes, M.T., Ferreira, M.P., Rocha, R., Soares, A., Zbyszewski, G.,
999 Moitinho de Almeida, F., 1979. Introduction à la géologie générale du Portugal, *Serv.*
1000 *Geol. Portugal*, 114p.
- 1001
- 1002 Ribeiro, A., Cabral, J., Baptista, R., Matias, L., 1996. Stress pattern in Portugal mainland
1003 and the adjacent Atlantic region, West Iberia. *Tectonophysics* 15(2): 641-659.
- 1004
- 1005 Roque, C., 2007. Tectonostratigrafia do Cenozóico das margens continentais Sul e
1006 Sudoeste portuguesas: um modelo de correlação sismostratigráfica. Departamento de
1007 Geologia, Universidade de Lisboa.
- 1008
- 1009 Rosas F.M., Duarte J.C., Terrinha P., Valadares, V., Matias, L., 2009. Morphotectonic
1010 characterization of major bathymetric lineaments in NW Gulf of Cadiz (Africa-Iberia
1011 plate boundary): insights from analogue modelling experiments. *Marine Geology* 261,
1012 33–47.
- 1013
- 1014 Rovere, M., Ranero, C. R., Sartori, R., Torelli, L., Zitellini, N., 2004. Seismic images
1015 and magnetic signature of the Late Jurassic to Early Cretaceous Africa-Eurasia plate
1016 boundary off SW Iberia. *Geophysical Journal International* 158(2): 554-568.
- 1017
- 1018 Sartori, R., Torelli, L., Zitellini, N., Peis, D., Lodolo, E., 1994. Eastern segment of the
1019 Azores-Gibraltar line (central-eastern Atlantic): an oceanic plate boundary with diffuse
1020 compressional deformation. *Geology* 22: 555-558.
- 1021

- 1022 Sella, G., Dixon, T., Mao, A., 2002. REVEL: A model for Recent plate velocities from
1023 space geodesy. *Journal of Geophysical Research*, 107.
- 1024
- 1025 Sillard, P., Altamimi, Z., Boucher, C., 1998. The ITRF96 realization and its associated
1026 Velocity field. *Geophysical Research Letters*, 25,(17), 3223-3226.
- 1027
- 1028 Somoza, L., Díaz-del-Río, V., León, R., Ivanov, M.K., Fernández-Puga, M.C., Gardner,
1029 J.M., Hernández-Molina, F.J., Pinheiro, L.M., Rodero, J., Lobato, A., Maestro, A.,
1030 Vázquez, J.T., Medialdea, T., Fernández-Salas, L.M., 2003. Seabed morphology and
1031 hydrocarbon seepage in the Gulf of Cádiz mud volcano area: Acoustic imagery,
1032 multibeam and ultra-high resolution seismic data. *Marine Geology*,(195), 153-156.
- 1033
- 1034 Srivastava, S. P., Roest, W. R., Kovacs, L. C., Oakey, G., Levesque, S., Verhoef, J.,
1035 Macnab, R., 1990. Motion of Iberia since the Late Jurassic: Results from detailed
1036 aeromagnetic measurements in the Newfoundland Basin. *Tectonophysics* 184(3-4):
1037 229-260.
- 1038
- 1039 Stich, D., Mancilla, F. de L., Pondrelli, S., Morales, J., 2007. Source analysis of the
1040 February 12th 2007, M_w 6.0 Horseshoe earthquake: Implications for the 1755 Lisbon
1041 earthquake. *Geophysical Research Letters* 34, 12.
- 1042
- 1043 Stich, D., Serpelloni, E., Mancilla, F.-L., Morales, J., 2006. Kinematics of the Iberia–
1044 Maghreb plate contact from seismic moment tensors and GPS observations.
1045 *Tectonophysics*, 426, 295-317.
- 1046

- 1047 Terrinha, P., 1998. Structural Geology and Tectonic Evolution of the Algarve Basin,
1048 South Portugal. Department of Geology. London, University of London.
1049
- 1050 Terrinha, P., Ribeiro, C., Kullberg, J.C., Rocha, R., Ribeiro, A., 2002. Compression
1051 episodes during rifting and faunal isolation in the Algarve Basins, SW Iberia. Journal of
1052 Geology, 110, p. 101-113.
1053
- 1054 Terrinha, P., Pinheiro, L.M., Henriot, J.-P., Matias, L., Ivanov, M.K., Monteiro, J.H.,
1055 Akhmetzhanov, A., Volkonskaya, A., Cunha, T., Shaskin, P., Rovere, M., 2003.
1056 Tsunamigenic-seismogenic structures, neotectonics, sedimentary processes and slope
1057 instability on the southwest Portuguese Margin. Marine Geology, 195,(1-4), 55-73.
1058
- 1059 Terrinha, P., Dias, R.P., Ribeiro, A., Cabral, J., 1999. The Portimão Fault, Algarve
1060 Basin, South Portugal. Comun. Inst. Geol. E Min., 86, pp. 107-120.
1061
- 1062 Torelli, L., Sartori, R., Zitellini, N., 1997. The giant chaotic body in the Atlantic Ocean
1063 off Gibraltar: new results from a deep seismic reflection survey. Marine and Petroleum
1064 Geology 14(2): 125-134.
1065
- 1066 Tortella, D., Torné, M., Pérez-Estáun, A., 1997. Geodynamic Evolution of the Eastern
1067 Segment of the Azores-Gibraltar Zone: The Goringe Bank and the Gulf of Cadiz
1068 Region. Marine Geophysical Researches 19(3): 211-230.
1069

- 1070 USGS, 2004. Shuttle Radar Topography Mission, 1 Arc Second scene
- 1071 SRTM_u03_n008e004, Unfilled Unfinished 2.0, Global Land Cover Facility,
- 1072 University of Maryland, College Park, Maryland, February 2000.
- 1073
- 1074 Van Rensbergen, P., Depreiter, D., Pannemans, B., Moerkerke, G., Van Rooij, D.,
- 1075 Marsset, B., Akhmanov, G., Blinova, V., Ivanov, M., Rachidi, M., Magalhaes, V.H.,
- 1076 Pinheiro, L.M., Cunha, M.R., Henriot, J.-P., 2005. The El Arraiche mud volcano field at
- 1077 the Moroccan Atlantic slope, Gulf of Cadiz. *Marine Geology*, 219,(1), 1-17.
- 1078
- 1079 Verdicchio, G., Trincardi, F., 2006. Short-distance variability in slope bed-forms along
- 1080 the Southwestern Adriatic Margin (Central Mediterranean). *Marine Geology* 234, 271-
- 1081 292.
- 1082
- 1083 Vizcaino, A., Gracia, E., Pallas, R., Garcia-Orellana, J., Escutia, C., Casas, D.,
- 1084 Willmott, V., Diez, S., Asioli, A., Danobeitia, J., 2006. Sedimentology, physical
- 1085 properties and age of mass transport deposits associated with the Marques de Pombal
- 1086 Fault, Southwest Portuguese Margin. *Norwegian Journal of Geology*, 86,(3), 177-186.
- 1087
- 1088 Voelker, A., Lebreiro, S., Schonfeld, J., Cacho, I., Erlenkeuser, H., Abrantes, F., 2006.
- 1089 Mediterranean outflow strengthening during northern hemisphere coolings: A salt
- 1090 source for the glacial Atlantic? *Earth and Planetary Science Letters*, 245, 39-55.
- 1091
- 1092 Zitellini, N., Chierici, F., Sartori, R., Torelli, L., 1999. The tectonic source of the 1755
- 1093 Lisbon earthquake and tsunamis. *Annali di Geofisica* 42(1).
- 1094

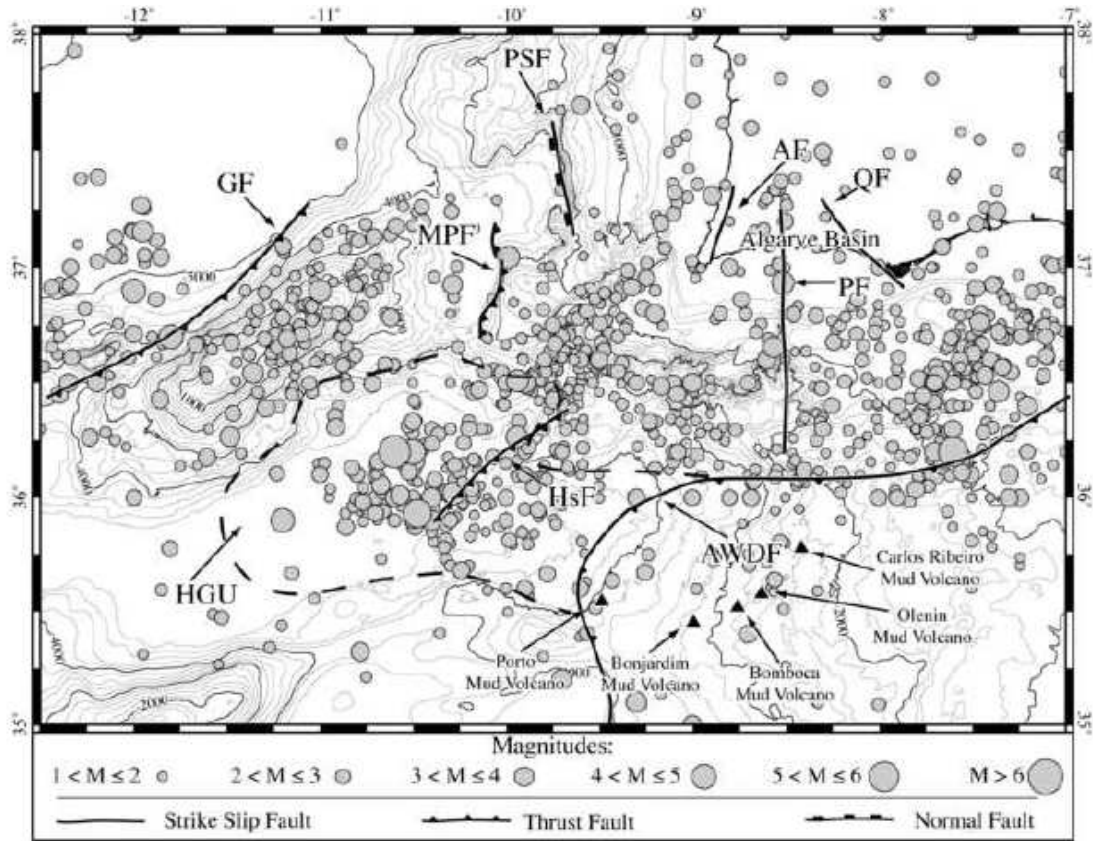
- 1095 Zitellini, N., Mendes, L. A., Cordoba, D., Danobeitia, J., Nicolich, R., Pellis, G.,
1096 Ribeiro, A., Sartori, R., Torelli, L., Bartolomé, R., Bortoluzzi, G., Calafato, A.,
1097 Carrilho, F., Casoni, L., Chierici, F., Corela, C., Correggiari, A., Della Vedova, B.,
1098 Gràcia, E., Jornet, P., Landuzzi, M., Ligi, M., Magagnoli, A., Marozzi, G., Matias, L.,
1099 Penitenti, D., Rodriguez, P., Rovere, M., Terrinha, P., Vigliotti, L., Zahinos Ruiz, A.,
1100 2001. Source of 1755 Lisbon Earthquake and Tsunami Investigated. *Eos Trans. AGU*,
1101 82, (26), 285, 290-291.
- 1102
- 1103 Zitellini, N., Ligi, M., Matias, L., Rovere, M., the Shipboard Scientific Parties, 2002.
1104 Voltaire 2002 Cruise Report. IGM-CNR Technical Report.
- 1105
- 1106 Zitellini, N., Rovere, M., Terrinha, P., Chierici, F., Matias, L., B. Team, 2004. Neogene
1107 Through Quaternary Tectonic Reactivation of SW Iberian Passive Margin. *Pure and*
1108 *Applied Geophysics*, 161, 565-587.
- 1109
- 1110 Zitellini, N., Gracia, E., Matias, L., Terrinha, P., Abreu, M.A., DeAlteriis, G., Henriet,
1111 J.P., Dañobeitia, J.J., Masson, D.G., Mulder, T., Ramella, R., Somoza, L., Diez, S.,
1112 2009. The quest for the Africa-Eurasia plate boundary west of the Strait of Gibraltar.
1113 *Earth and Planetary Science Letters*, 280, 1-4, pp: 13-50.
- 1114
- 1115 **Figure captions**
- 1116 Fig. 1. Location and main morphological features of the study area. Inset shows the
1117 geotectonic location of the area and the relative motions of the Eurasia, Nubia and
1118 North America lithospheric plates in mm/year. Triangles show location of mud
1119 volcanoes.



1120

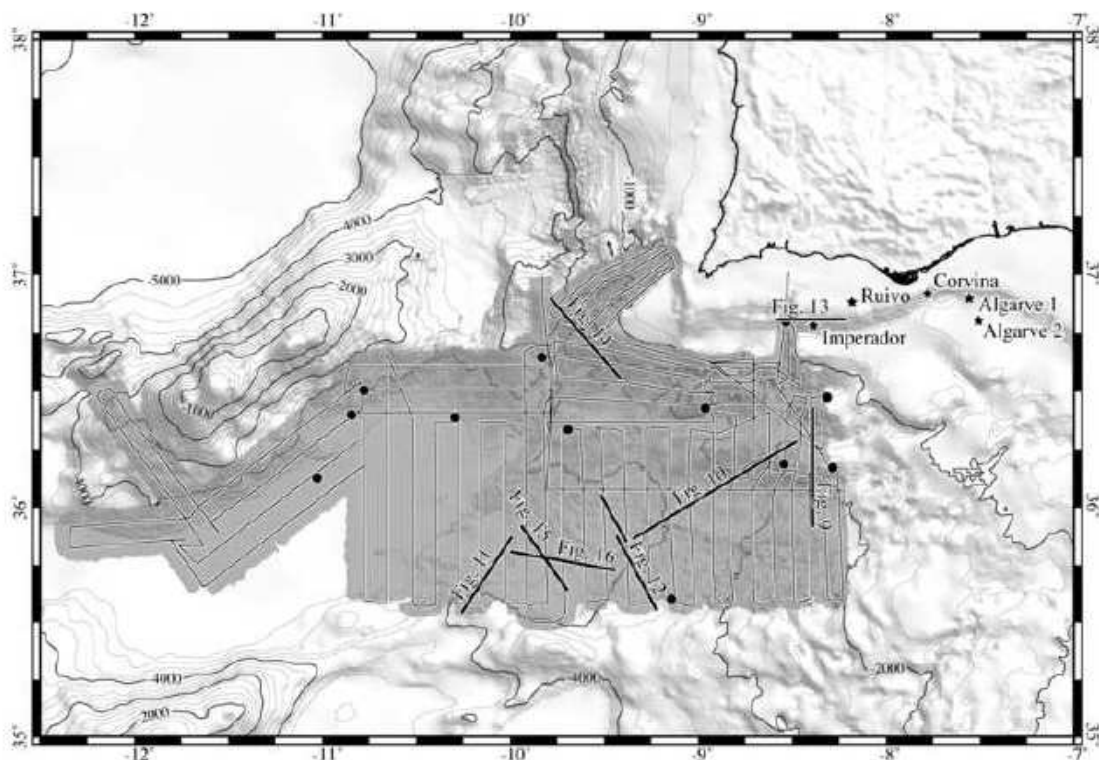
1121

1122 Fig. 2. Seismicity of the study area, the main faults and boundaries of the Accretionary
 1123 Wedge of the Gulf of Cadiz and Horseshoe Gravitational Unit as mapped in previous
 1124 works (Sartori et al., 1994; Torelli et al., 1997; Gutscher et al., 2002; Gràcia et al., 2003;
 1125 Terrinha et al., 2003; Iribarren et al., 2007). AF- Aljezur Fault; AWDF- Accretionary
 1126 Wedge Deformation Front; GF- Gorringe Fault; HGU- Horseshoe Gravitational Unit;
 1127 HsF- Horseshoe Fault; MPF- Marquês de Pombal Fault; PF- Portimão Fault; PSF-
 1128 Pereira de Sousa Fault; QF- Quarteira Fault; Triangles show the location of mud-
 1129 volcanoes.



1130

1131 Fig. 3. Map showing the acquisition track lines of the MATESPRO multibeam
 1132 bathymetry and the position of the seismic reflection lines shown in this work. Circles
 1133 indicate location of the Sound Velocity Profiles performed. Location of oil prospecting
 1134 wells (stars) is also shown. Altimetry data derived from SRTM (USGS, 2004).



1135

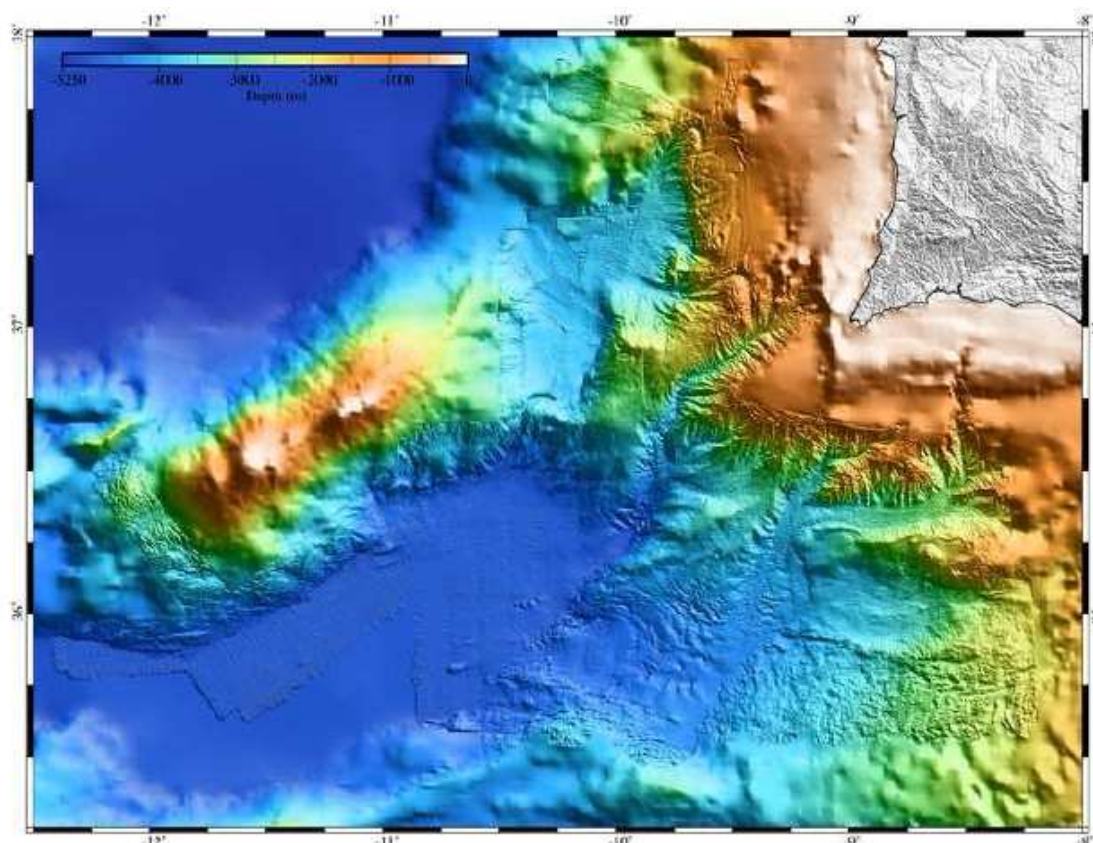
1136 Fig. 4. Multibeam bathymetry map of the MATESPRO study area, offshore SW Iberia.

1137 Topography of onshore area also shown as shaded relief with a maximum of 902 m.

1138 Mercator projection, datum WGS84. PARSIFAL bathymetry of the Marquês de Pombal

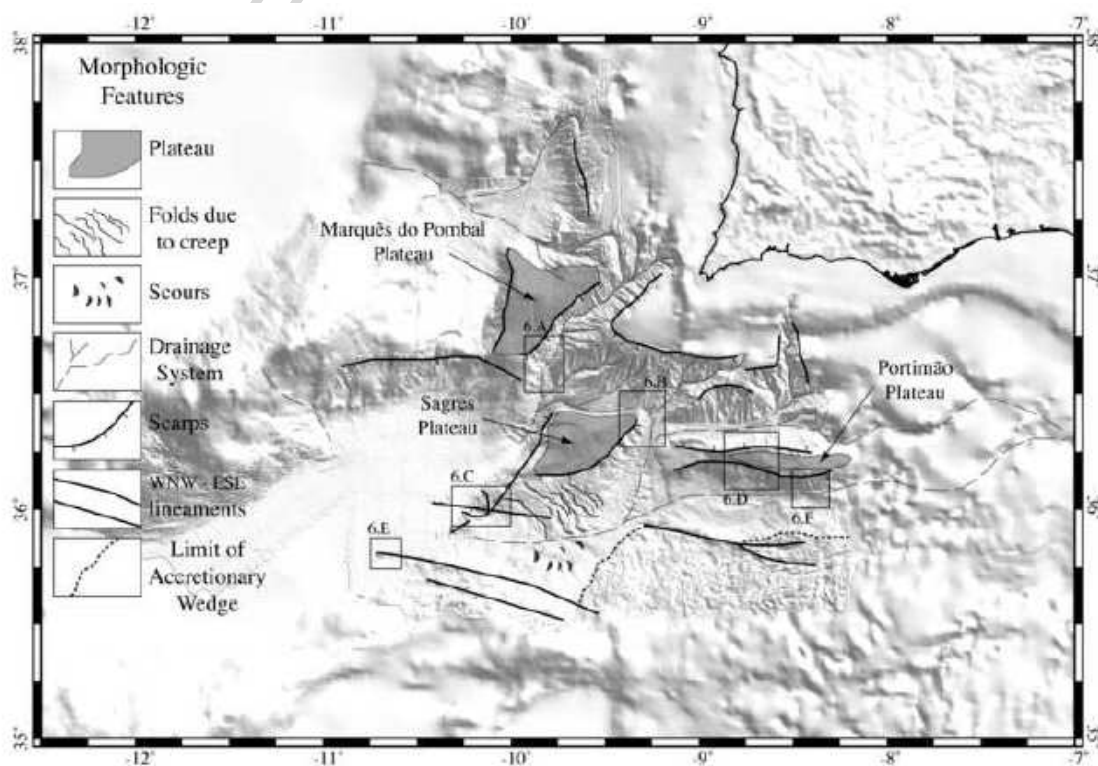
1139 area and Pereira de Sousa escarpment published by Gràcia et al. (2003). Bathymetry for

1140 other offshore areas and onshore altimetry is taken from Gebco (IOC et al., 2003).



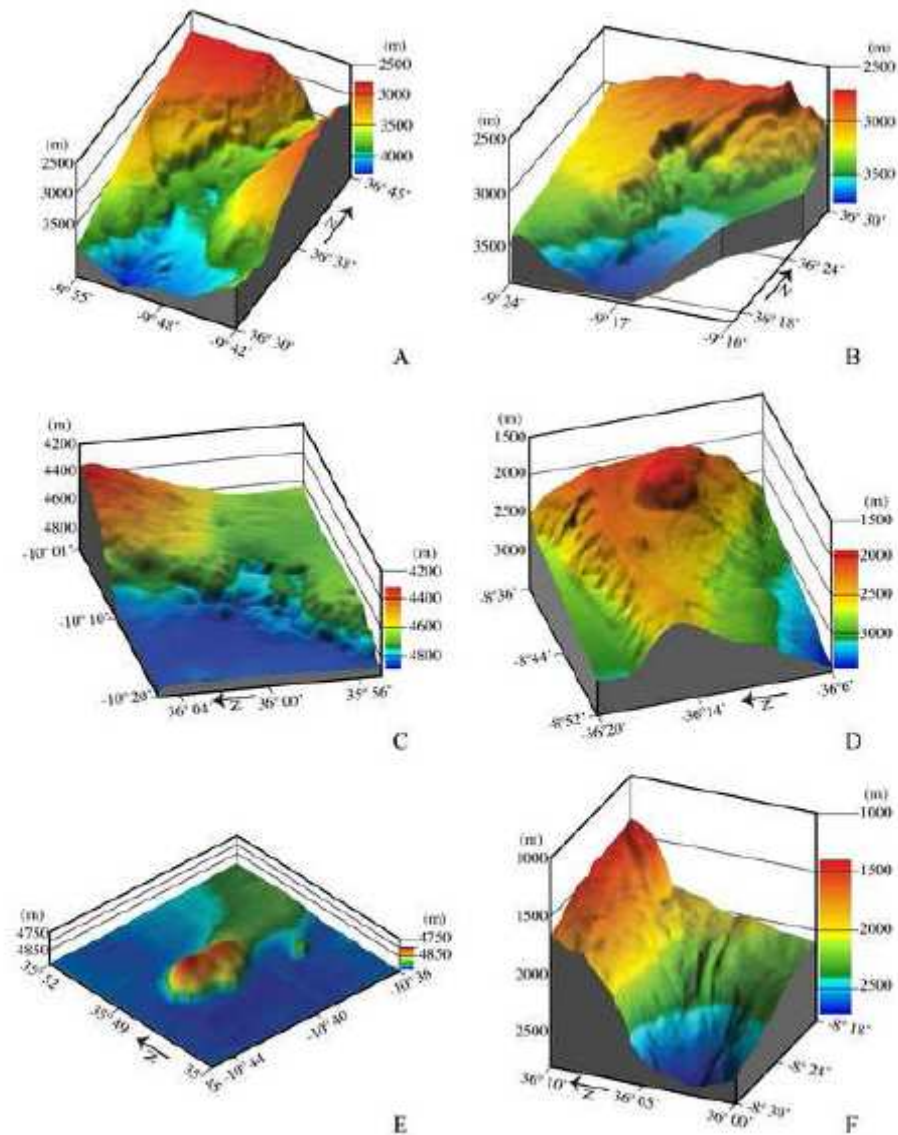
1141

1142 Fig. 5. Interpretative sketch of the morphology of the study area. 6.A to 6.F, location of
 1143 the features imaged in 3D in Fig. 6.



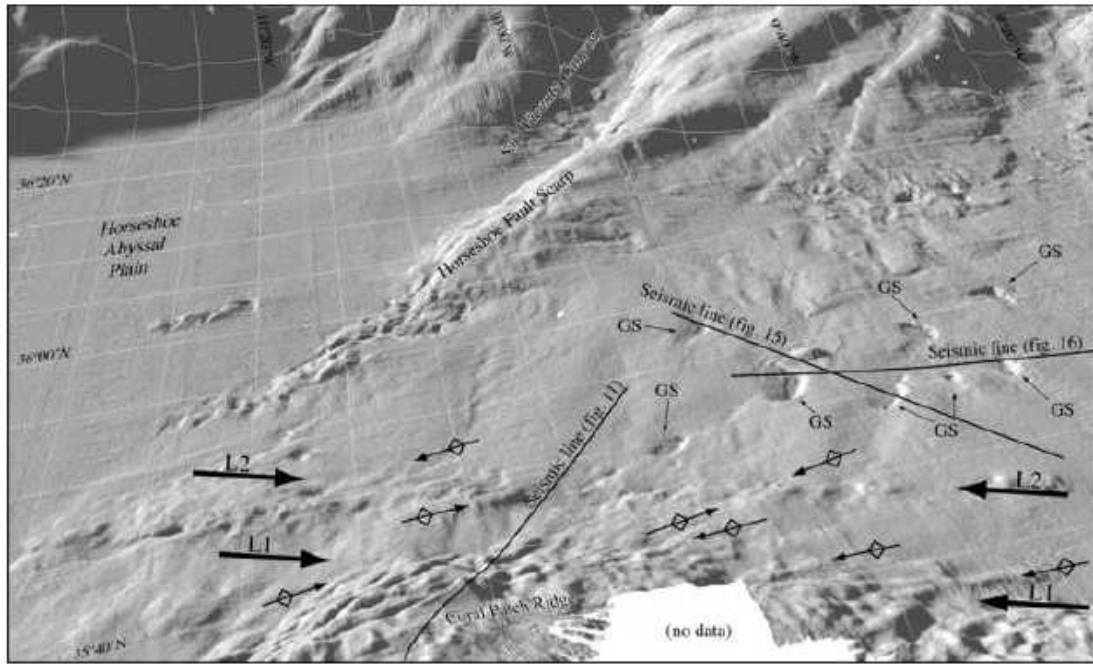
1144

1145 Fig. 6. 3D block diagrams of selected morphologic features of the study area. Images
1146 made from MATESPRO multibeam data presented in this work. A) Slide scar on the
1147 western flank of the S. Vicente canyon. B) Slide scar on the western flank of the Sagres
1148 valley. C) Slide scar on the Horseshoe fault scarp at the intersection with the WNW-
1149 ESE trending lineaments. D) D. Carlos salt diapir protruding through the top of the
1150 Portimão Bank (cf. with Fig. 10 for internal structure). Note the incisions on both flanks
1151 of the plateau, mainly on the northern side. E) E-W oriented hill in the Horseshoe
1152 Abyssal Plain sitting on top of one of the WNW-ESE trending lineaments. F) E-W
1153 trending channel at the foot of the Portimão Bank, whose structure in depth is imaged in
1154 MCS profile in Fig. 9. See text for detailed description.



1155

1156 Fig. 7. Shaded relief image (perspective view) of the Giant Scours (GS), L1 and L2
 1157 WNW-ESE trending lineaments (interpreted as strike slip faults, max. total length
 1158 250km, see Fig. 11) and associated en echelon folds on sea floor recent sediments
 1159 indicating dextral strike-slip movement component on the faults. Approximate depth
 1160 4000m, confer with Figs. 1 and 4. Position of seismic lines in Figs. 11, 15 and 16 is also
 1161 shown. Detail of the en echelon folds on L1 in the Horseshoe Abyssal Plain is shown in
 1162 Fig. 6E.



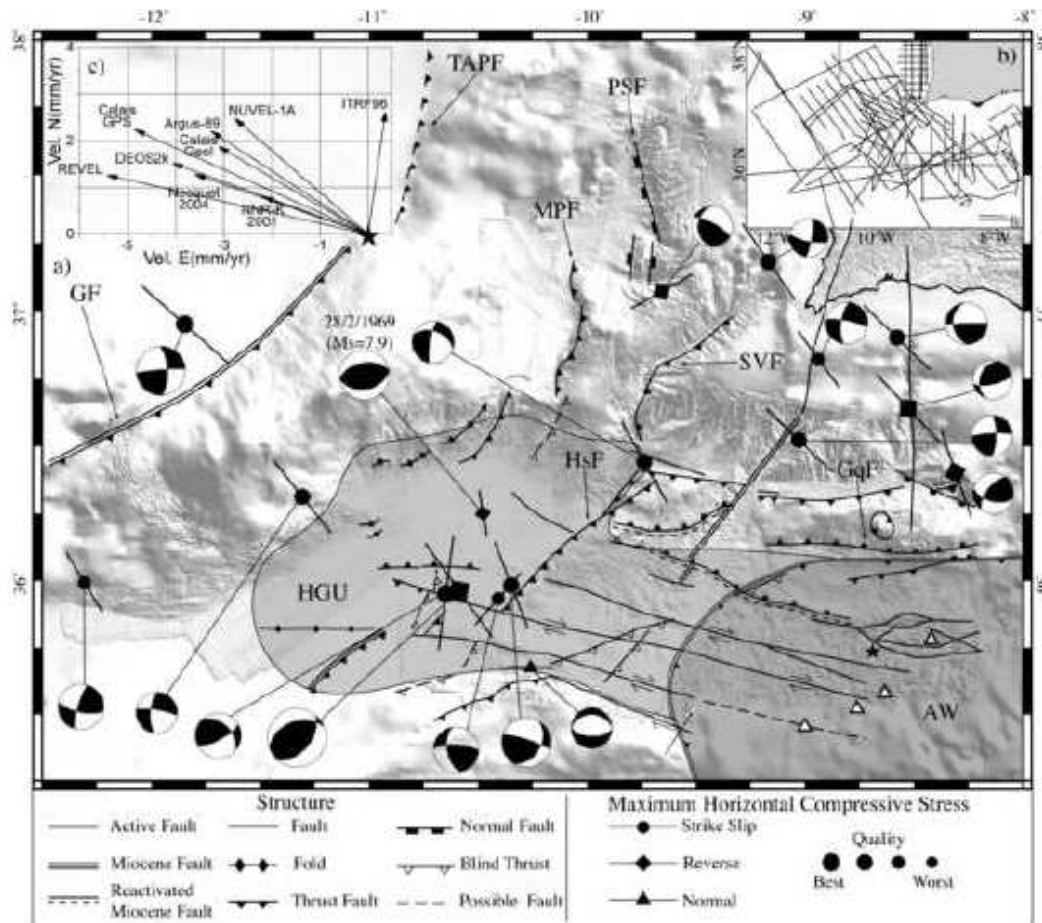
1163

1164

1165 Fig. 8. A) Structural map of the study area with a compilation of stress indicators and
 1166 focal mechanisms. Stress indicators computed from earthquake focal mechanisms and
 1167 faults from interpretation of MCS profiles dataset shown in inset b). The size of the
 1168 stress indicators is proportional to their quality. Note that position of mud volcanoes
 1169 (white triangles) are in close spatial association with interpreted WNW-ESE dextral
 1170 strike-slip faults. Fault names from published work as in Fig. 2. PbF- Portimão Bank
 1171 fault; SVF- S. Vicente Fault; TAPF- Tagus Abyssal Plain Fault.

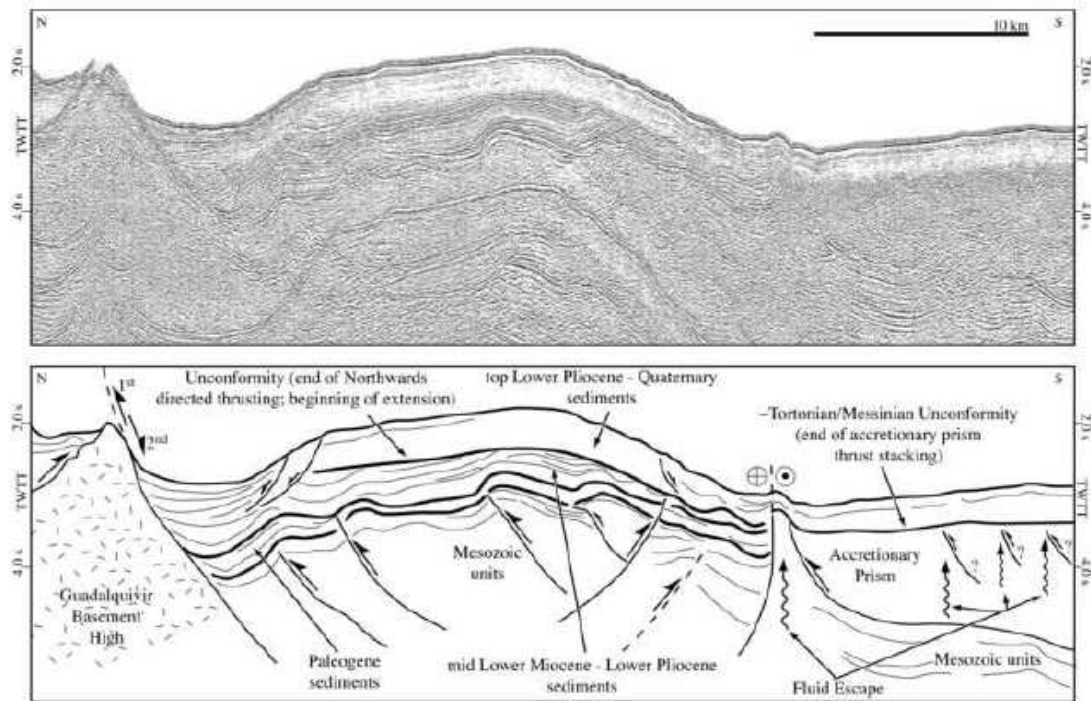
1172 B) Location of the MCS profiles used in this work.

1173 C) Plate kinematic data taken from various indicated sources indicated in the text. Black
 1174 star shows position of computed movements of Nubia with respect to Iberia.



1175

1176 Fig. 9. Multi-channel seismic line VOLTAIRE 3 and line drawing interpretation. The
 1177 Guadalquivir basement high of Carboniferous age is bound by a NW-SE trending
 1178 Mesozoic extensional fault, reactivated as a reverse fault (1st movement) that resumed
 1179 its extensional movement in late Miocene through Present times (see text for discussion,
 1180 for location of line see Fig. 1). The topographic bulge on top of the strike-slip fault is
 1181 imaged in 3D in Fig. 6F.



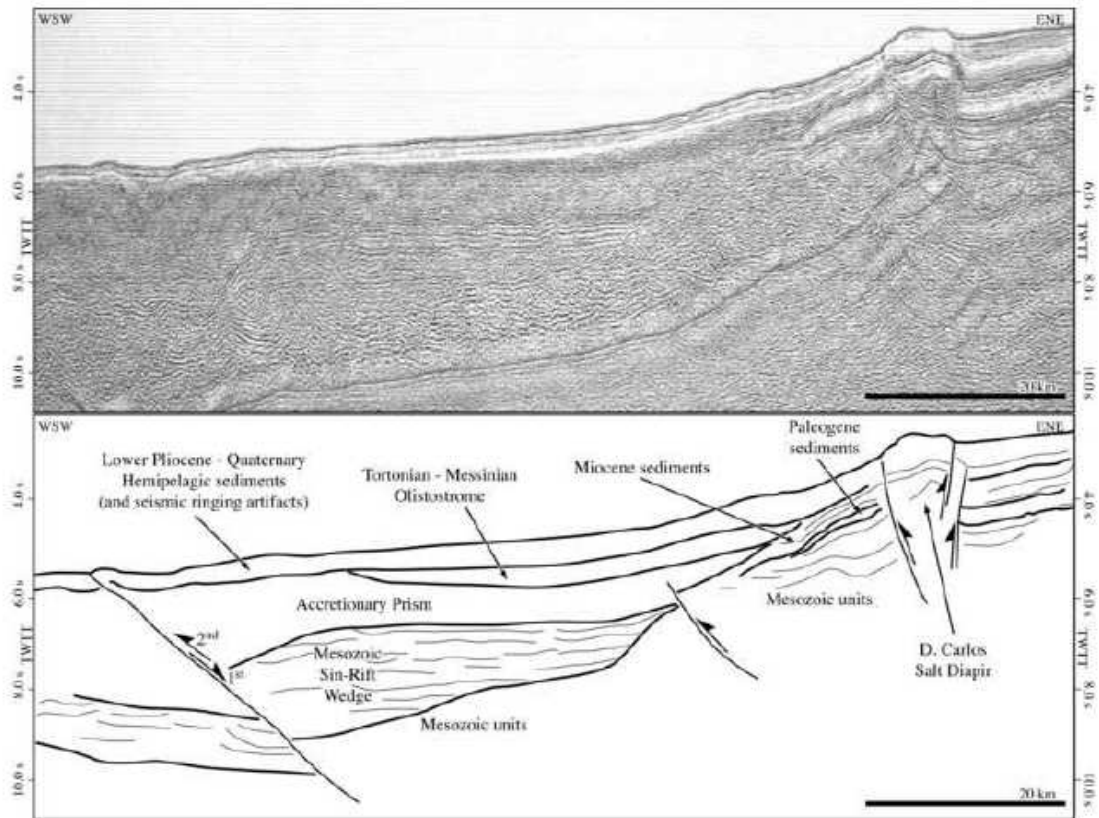
1182

1183 Fig. 10. Segment of multi-channel seismic line ARRIFANO 92-04 and line drawing

1184 interpretation. 1st and 2nd movements on main faults are of Jurassic-Cretaceous age and

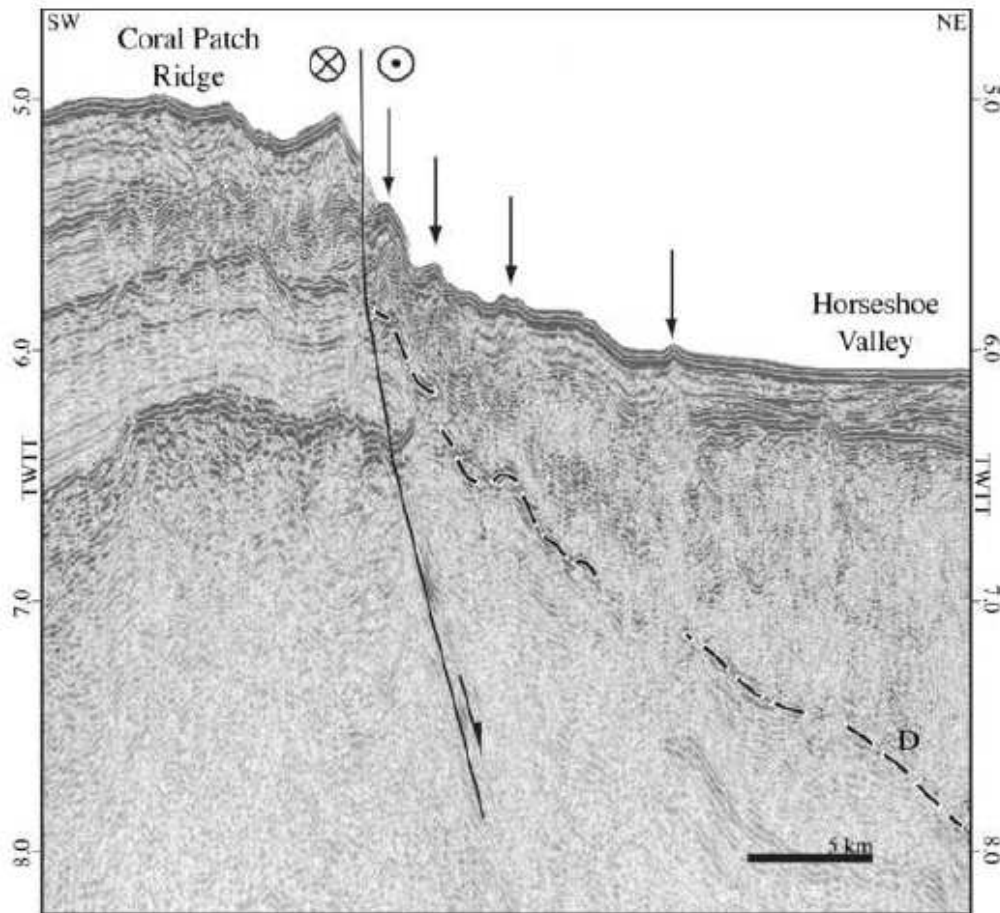
1185 latest Miocene through Present, respectively. For location of seismic line see Fig. 3. The

1186 D. Carlos salt diapir 3D topography is shown in Fig. 6D.



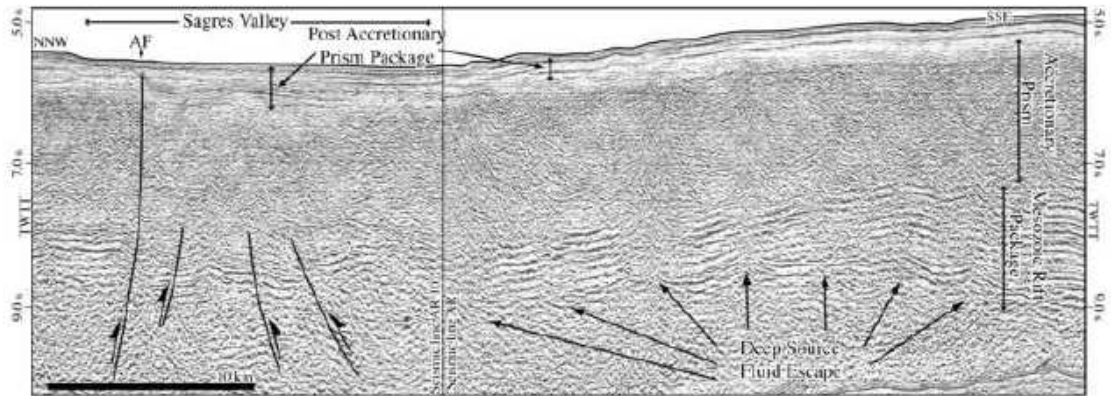
1187

1188 Fig. 11. Segment of multi-channel seismic profile IAM-3 at the contact between the
 1189 Coral Patch Ridge (CPR) and the Horseshoe valley. Arrows point to folds in recent
 1190 sediments on the seafloor as imaged on the MATESPRO bathymetry (see Figs. 3 and
 1191 7). Note that these faults cut across seismic discontinuity D that outlines the
 1192 decollement of the seismic chaotic facies.



1193

1194 Fig. 12. Segment of multi-channel seismic line ARRIFANO 92-10 showing the deep
 1195 origin of fluidized sediments breaching through the Mesozoic rift units and accretionary
 1196 prism. Also note that the most recent unit is not involved in the thrust stacking tectonics
 1197 of the accretionary wedge (see text for discussion, for location of line see Fig. 3). The
 1198 steeply dipping north westernmost fault is the Aljezur fault bounding the deposits of the
 1199 Sagres valley. Note that the chaotic body under the Sagres valley also has imbricated
 1200 horizons but has no influence on the seafloor morphology (see text for discussion).



1201

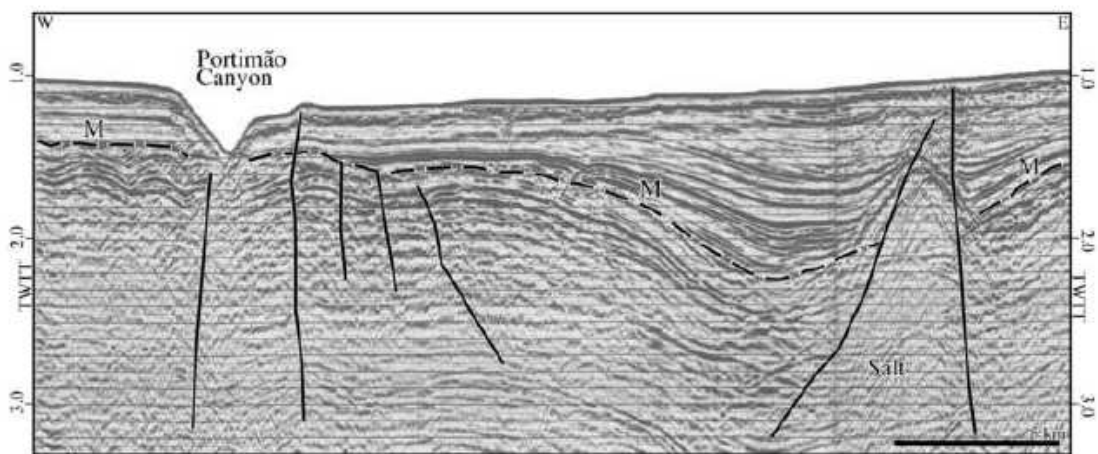
1202 Fig. 13. Segment of multi-channel seismic line perpendicular to the Portimão canyon.

1203 Note that the Lower Miocene unconformity (M) truncates the folds that resulted from

1204 tectonic inversion on both sides of the Portimão canyon fault. However, mild

1205 deformation associated with this fault is visible on the eastern side of the fault and

1206 canyon. The salt-wall shown in the east of the profile also affects the recent sediments.



1207

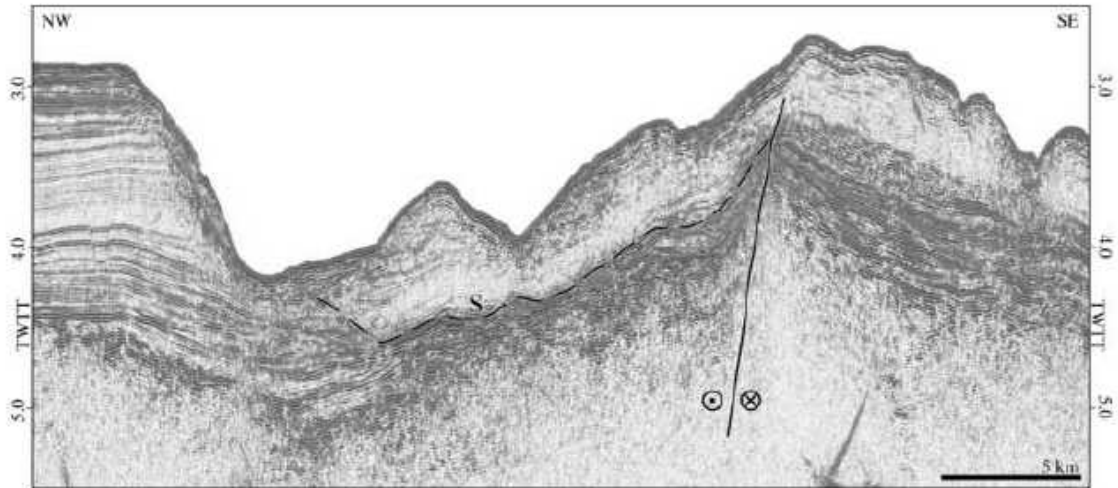
1208 Fig.14. Segment of multi-channel seismic line perpendicular to the S. Vicente canyon.

1209 Note the main fault controlling the position of the eastern flank of the canyon. This is a

1210 steep fault, possibly en echelon with the Messejana dyke fault (see text for description).

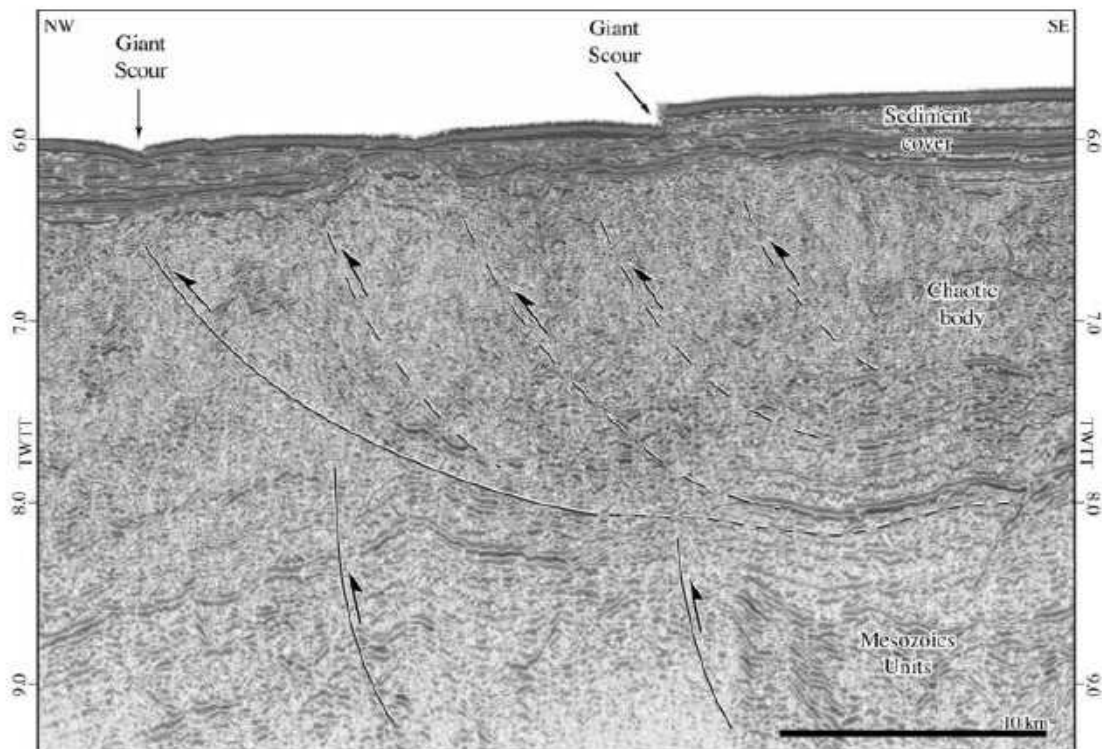
1211 Sediments on both sides of the fault are tilted and deformed including seismic reflector

1212 S, which is interpreted as a paleo-canyon bottom.



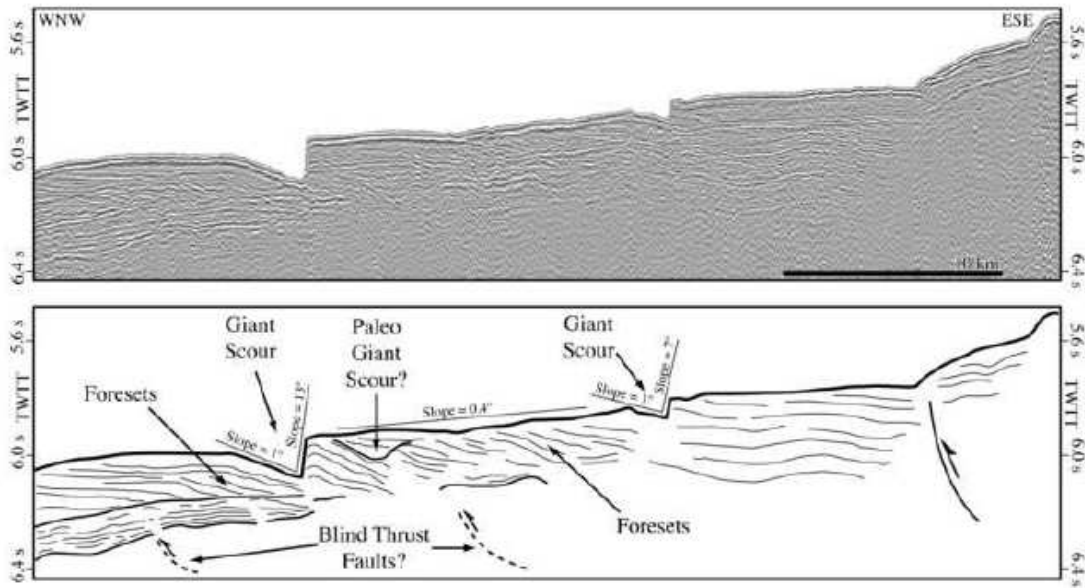
1213

1214 Fig 15. Multi-channel seismic reflection profile across the Giant Scours. For location of
 1215 the lines see Figs. 3 and 7. Seismic line IAM-4E shows the existence of stacked blind
 1216 thrusts with present activity underneath the Giant Scours in the Sagres valley.



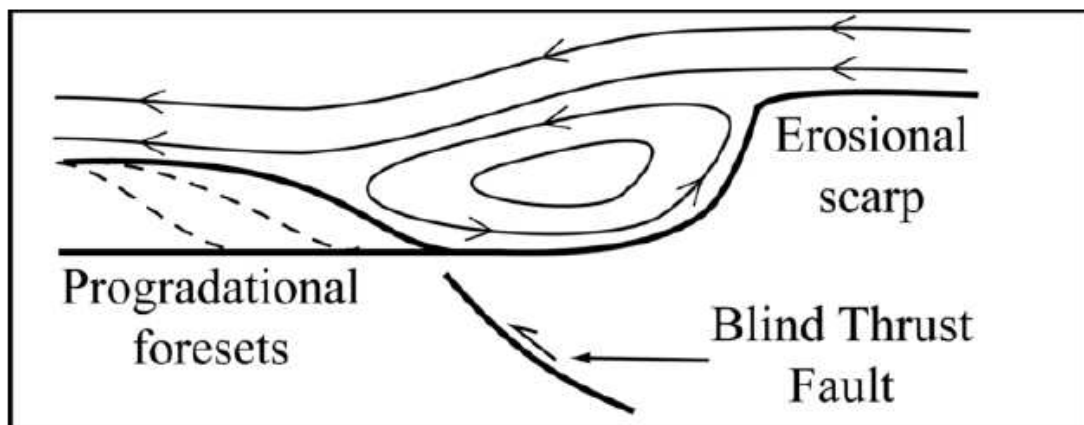
1217

1218 Fig. 16. Single-channel seismic line PSAT246 across two scours and line drawing
 1219 interpretation. Note the erosive character of the escarpments and the sediments
 1220 prograding towards the escarpment. For location see Figs. 3 and 7.



1221

1222 Fig. 17. Sketch of the effect of bottom currents on the retreat of the scarp and
 1223 simultaneous progressive sedimentation of the progradation foresets. Scarp initially
 1224 formed by uplift of hanging-wall on top of a blind thrust (see text for discussion).

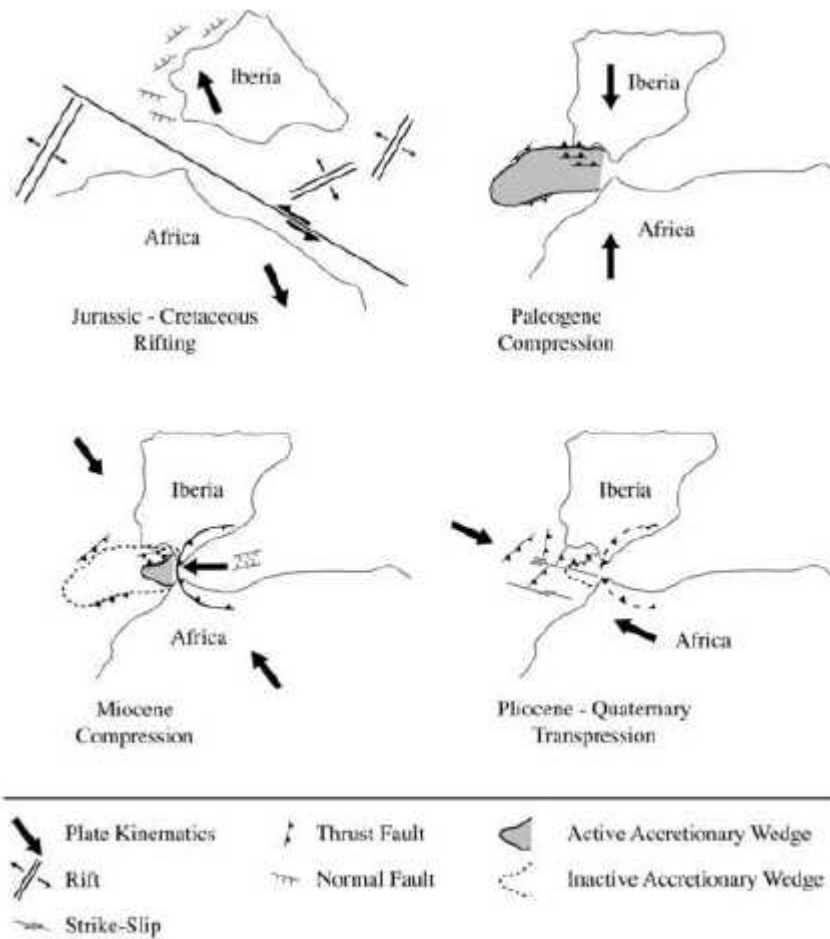


1225

1226

1227 Fig. 18. Schematic tectonic evolution of the structure of the Gulf of Cadiz. In this
 1228 simplified interpretation it is proposed the formation of an accretionary wedge (or
 1229 thrust belt) that extended from Gibraltar across the Horseshoe Abyssal Plain during the
 1230 latest Cretaceous – Paleogene compression. A second accretionary wedge formed (after

1231 Gutscher et al., 2002, or imbricate unit after Iribarren et al., 2007) during the Gibraltar
 1232 orogenic arc westward overthrusting in Miocene times. In Pliocene-Quaternary times
 1233 this accretionary wedge severely diminished its activity, the WNW-ESE dextral strike-
 1234 slip faults formed and westward directed thrust increased along faults on the southern
 1235 part of the West Portuguese Margin. See text for detailed discussion.



1236

1237

	ARRIFANO	IAM	Voltaire	TTR-14
Year	1992	1993	2002	2004
Vessel	R/V OGS Explora	Geco Sigma	R/V Urania	R/V Prof Logachev
Reference	Sartori et al. 1994	Banda et al. 1995	Zitellini et al., 2002	Kenyon et al., 2006
Seismic source	32 Airguns (80 litres max.)	30 Airguns (125 litres max.)	2 GI guns	1 Airgun (120 bar)
Shooting Interval	50 meters	74 meters	50 meters	10 seconds (aprox 30 metres)
Sample Interval Recorded	1 ms	4 ms	1 ms	1 ms
Number of channels	120	192	48	1

Resampling	4 ms	8 ms	2 ms	1ms (no resampling)
Signal Processing	Spiking deconvolution Spherical divergence correction NMO correction Finite-difference wave-equation migration Time variant bandpass frequency filter	NMO correction Kirchoff migration (constant velocity 1700m/s) AGC, 500 ms time gate	Trace editing Shot delay removal Amplitude recovery Predictive deconvolution Velocity analysis every 200 CMPs NMO correction Stack Band-pass-frequency filtering Time migration using stacking velocities	Static correction Spiking deconvolution Spherical divergence correction Butterworth bandpass filtering (20-60-180-240 Hz)

1238

ACCEPTED MANUSCRIPT